



# Development of agricultural waste/recycled plastic/waste oil bio-composite wallpaper based on two-phase dye and liquefaction filling technology

Dingtian Xiao<sup>1</sup> · Zhifeng Yu<sup>1,2</sup> · Shan Qing<sup>1</sup> · Shunlin Du<sup>3</sup> · Huaqiang Xiao<sup>3</sup>

Received: 30 July 2019 / Accepted: 25 November 2019 / Published online: 12 December 2019  
© Springer-Verlag GmbH Germany, part of Springer Nature 2019

## Abstract

In this paper, a complete biomass composite processing system based on agricultural waste powders, recycled plastics, and waste oil is proposed. The wood-colored wallpaper, the green wallpaper, and the blue wallpaper are produced by this processing system. These wallpapers are new products with low cost, high added value, and environmental friendliness. These wallpapers have also been systematically tested. Based on the analysis of test results, a 3D model of material formation mechanism, liquefaction filling technology, and hybrid network model construction technology are obtained. The experiment found the reasonable RLDPE and RLLDPE ratio (1:0.26), the reasonable ratio of biomass to specialty solvents (1:1.5), the reasonable dose of the solid dye (3%), and the reasonable concentration of dye solutions. Wood-colored bio-composite wallpaper products have a smooth surface, wood color ( $\Delta E = 36.7$ ), natural aroma, and good comprehensive mechanical properties (tensile strength 9.255 MPa; elongation at break 20.998%; Young's modulus 2229.475 MPa). The processing system and wallpaper products in this article not only promote the plastic recycling economy and sustainable agricultural development but also provide new channels for the development of waste oil reuse and new ideas for the development of high value-added biocomposite materials.

**Keywords** Green products · Garbage reuse · Novel dyeing technology · Processing system

## Introduction

Since 1950, 50% of plastic waste has been landfilled on land and the rest has entered the ocean (d'Ambrières 2019). Eight million tons of marine debris appears in the ocean per year, some of which form a 1.6-million-square kilometer Pacific landfill (Cheranov et al. 2019). Marine debris not only causes harm to people through the food chain (Chatterjee and Sharma 2019) but also creates ecosystem deterioration and a tremendous “tragedy of the commons” in oceans and rivers (Barnes

2019). On March 27, 2019, The European Parliament voted to pass a ban on disposable plastic products to recycle 90% of plastic waste. The wallpaper product developed in this article is in conformity with the concept of plastic recycling economy (Defruyt 2019).

China's gas pollution caused by straw burning is one of the biggest threats to Chinese health (Qu et al. 2012), which leads to the premature death of 1.2 million people (Yang et al. 2013). Straw burning has played a big role in air pollution as a seasonal source (Zhang et al. 2014). It produces harmful substances such as air pollutants (CO, NH<sub>3</sub>, NO<sub>x</sub>, SO<sub>2</sub>, NMHC), particulate matter, and smog (Jain et al. 2014) on the one hand and destroys the soil by injuring the microorganisms in the soil such as bacteria on the other hand (Xiue 2003). The cultivation of rice, wheat, and corn in China is regional and intensive, which leads to a large concentration of waste (Cao et al. 2008). Direct combustion of these wastes causes smog (Wang et al. 2009) and the abandonment of wastes causes water's eutrophication (Yang Chunhe 2005). Further technological innovations in waste recycle fields are necessary (Wei et al. 2011).

As a kind of novel material with low density and eco-friendly nature, biomass composites have been extensively

---

Responsible editor: Ta Yeong Wu

✉ Dingtian Xiao  
1350369663@qq.com

- <sup>1</sup> School of Metallurgical and Energy Engineering, Kunming University of Science and Technology, Kunming 650000, Yunnan, China
- <sup>2</sup> Faculty of Civil Engineering and Mechanics, Kunming University of Science and Technology, Kunming 650500, China
- <sup>3</sup> Wukun Steel Co. Ltd, Kunming, Yunnan, China

studied by many scholars (Saba et al. 2014) (Ku et al. 2011). The wood-plastic composites link the timber industry to the plastics industry (Clemons 2002). Some scholars focus on the pretreatment of biomass. For example, Liu (Liu et al. 2014) used the wood flour pretreated by the nitric acid–ethanol method to produce composites. Other scholars concentrate on the effects of filler loading levels. For example, Kaymakci (Kaymakci and Ayrimis 2014) used three parts of sawdust flour with a mass fraction of 30%, 40%, or 50%, respectively, to mix with the polypropylene to produce composites. The development of wood-plastic composite leads to deforestation. So other biomass fillers such as jute fibers and banana fibers have been studied. Patel (Patel et al. 2012) used epoxy resins as matrix and jute fibers as filler to develop novel composites. Pothan (Pothan et al. 1997) developed composites using banana staple fiber and polyester. Directly using agricultural products as fillers makes the cost of raw material higher. Further surface modification and the addition of expensive additives such as MAPP and MAPE (Patel et al. 2012) (Özmen 2012) have doubled the cost. The combination of the above reasons has led to poor feasibility of these materials.

Poly-lactic acid biomass composite has been widely studied by many scholars using different processing methods. Cecchi (Cecchi et al. 2019) prepared composite with mussel shell powders and PLA by directly stirring the mixture at constant temperature (180 °C) for 15 min. Arena (Arena et al. 2011) prepared PLA/fluorohectorite/montmorillonite composites by melt-blending method. Some scholars have studied other biomass composite such as PHBV/hemp composite (Miller et al. 2013). PLA and PHBV are obtained from starch by a multi-step ester conversion reaction which makes them very expensive. This reason leads to high cost of materials. As the most abundant raw material, straw has been widely studied in the packaging industry (Gao et al. 2007) (Lin et al. 2011) and many patented technologies have emerged (Wang 2001) (Yin 2013). Although these studies are meaningful, their products are low value-added products. Some scholars pay attention to the particle size of straw (Lowa et al. 2017), while

others pay attention to the content of additives such as MAPE (Tajeddin and Ansari 2017). These scholars have not considered that the thinner the straw, the higher the cost. The plastic contamination caused by MAPE itself has also been ignored. This paper introduces a new technology for the development of high value-added new-scented colored biomass composite wallpaper using agricultural waste powders (AWP) and recycled plastics as raw materials. The high level of waste recycling, the wide adaptability of raw materials, and the harmless process make this technology environmentally friendly and economical.

## Material and methods

### Materials

#### Detailed description of ingredients

**Agricultural waste powders (AWP)** Many scholars use a single plant fiber as filler to design the process, which lacks practicality and economy. Grain planting bases produce many types of agricultural waste, which requires the process to have a wide adaptability to raw materials. In this paper, a biomass composite process suitable for the characteristics of the planting base's agricultural waste is studied. As shown in Fig. 1 and Table 1 below, the composition of the mixed powders used in this paper and the situation of crops planted in the Langfang planting base. The AWP is a mixture of agricultural wastes mainly composed of wheat straw. The other components are barley straw, discarded bamboo leaves, rice stems, rice leaves, rice husks, corn stems, corn cob, and corn leaves. These raw materials are provided from Langfang Yikang Flour Co., Ltd. (Langfang, China) which is a grain planting base. The powders are produced by the joint factory of the Yikang company and Kunming University of Science and Technology (KUST).

These agricultural wastes have been processed in three stages. First, they are collected from farmland by agricultural machines and sent to the large pulverizer. Then they are sent to a large grinder for grinding after being washed and dried.

**Fig. 1** The pie chart of the composition of the mixed powder used in this paper and the pie chart of the situation of crops planted in the Langfang planting base

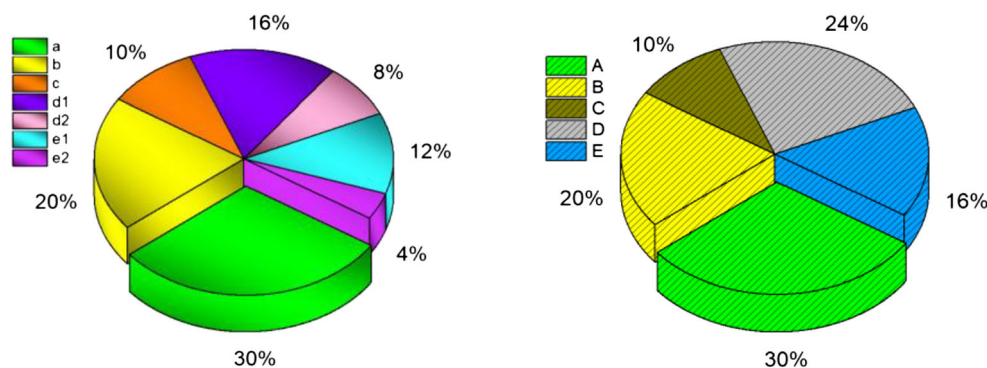


**Table 1** The composition of the mixed powder used in this paper and the situation of crops planted in the Langfang planting base

| Agricultural waste types                   | Proportion (%) | Plant species     | Proportion (%) |
|--|----------------|-------------------|----------------|
| Wheat straw (a)                            | 30             | Wheat field (A)   | 30             |
| Barley straw (b)                           | 20             | Barley field (B)  | 20             |
| Discarded bamboo leaves (c)                | 10             | Bamboo forest (C) | 10             |
| Rice stems and leaves (d1)/rice husks (d2) | 16/8           | Rice field (D)    | 24             |
| Corn stems and leaves (e1)/corn cob (e2)   | 12/4           | Corn field (E)    | 16             |

Finally, they are sent to a jet mill for further grinding to refine the particles. The obtained powders are dried again and stored in a warehouse. The large pulverizer has large cutting gears and blades that process the bulk material into small pieces. The jet mill uses multiple high-pressure gas streams to grind coarse particles into fine particles at the junction and separates them by powerful centrifugation of the stage turbine.

**Recycled plastic** Recycled plastics used in this article were supplied by Wang Brothers recycled plastic Co. Ltd. (Yunnan, China). These products are produced by the joint laboratory of the company and KUST. This company has a complete set of patented technology and supporting equipment. The waste plastics are washed and dried after classification and collection. The pretreated waste plastic is sent to a pulverizing device. Pulverized plastic powders are sent to the melting furnace after being washed twice and dried again. The melted plastic is extruded into wires after passing through a decontaminating device and a decoloring device. The company has a patented complete decontaminating device with multiple processes such as melt filtration, melt centrifugation, and electrostatic separation to remove solid impurities and plastic impurities. The patented decolorizing device has a melt extraction and a multi-stage porous adsorption column to remove residual pigment impurities. The wires become oval recycled plastic granules after a cold air hot cutting process. According to the processing technology and technical data of different products of this factory, the products of the factory can be divided into three grades (Table 2).

Recycled linear low-density polyethylene (LLDPE) is the third class (powdery, MFI 2 g/10 min, density 0.918 g/cm<sup>3</sup>); recycled low-density polyethylene (LDPE) is the second class (2–3 mm, MFI 1.6 g/10 min, density 0.923 g/cm<sup>3</sup>).

**Two kinds of raw materials recycled from the waste oil**

Purified waste oil and solid waste oil powders are provided by Kunming Lidian Co., Ltd. (Yunnan, China). The patented technology for waste oil processing has four steps. The first step is to collect enough waste oil in the restaurant’s waste barrels and sewers. The second step is to use boilers for multiple boils and filter screens for multiple filtrations. The third step is to add sodium hydroxide and calcium hydroxide into the solution for alkali refining and wash the mixture with water. The fourth step is to decolorize the solution with activated clay and activated carbon. After these four steps, the purified waste oil is obtained. The saponin produced in the alkali refining process and the collected waste solid animal oil are sent to a heating furnace and mixed in a molten state. The furnace temperature is controlled at 100–120 °C and the process of heating and stirring the mixture is continued for 1–2 h. The homogeneous mixture is sent to refrigeration equipment. The refrigerating temperature is set at –10 °C to –5 °C and the refrigerating time is 24 h. The obtained mixture is finally frozen into pieces and sent to a freeze mill for grinding into solid waste oil powders. After coming out of the twin-screw extruder, the solid oil is more likely to solidify than the liquid plastic. The easily solidified component facilitates the formation of the composite as curing agent.

**Other reagents** Erioglaucline disodium salt (5000 mesh) is provided by Macleans Co., Ltd. (Shanghai, China). HLA-TiO<sub>2</sub> (anatase-type titanium, hydrophilic, and lipophilic anatase-type, 99.8% metals basis, 5–10 nm), calcium gluconate (USP level, 500 mesh), ultrafine kaolin (K100132, 5um), lauryl methacrylate (LMA) (96%, 500 ppm MEHQ stabilizer) are provided by Aladdin Co. Ltd. (Shanghai, China).

**Table 2** Classification of the recycled plastics

| Product category              | Source of raw materials                | Value (percentage of new plastic prices) (%) |
|-------------------------------|--|--|
| First-class recycled plastic  | Leftover material; bottom material     | 70–80  |
| Second-class recycled plastic | Plastic used once                      | 50–70  |
| Third-class recycled plastic  | Plastic used twice and more than twice | 30–50  |

## Ingredients and classification

The reagents and substances used in the experiment are listed in Table 3.

## The main processing equipment

The composite in this paper is processed by means of twin-screw extrusion compounding. The compounding process is finished by SY-6217-ZB laboratory twin-screw extruder program-controlled type (Shiyan, Dongwan, China). The screw of twin-screw extruder is 40CrNiMo chrome-molybdenum alloy special tool steel. The screw has a feed section, a compression section, a metering section, and a mixing head. The nitride layer depth is 0.4–0.7 mm and the nitride hardness is HRC55–60. The screw also has a polished hard chrome plating. The screw diameter is 30 mm and L/D is 40:1. The twin screw system is a modular spiral combination and the barrel is multi-stage combined. This machine is equipped with a PLC programmable controller and a 10-in. color touch screen display which can adjust speed and temperature.

The granules of biomass composites are processed by SY-6219 laboratory cast film machine (Shiyan, Dongwan, China) to produce films. The cast film machine consists of two main parts. One is a single-screw extruder and the other is a cast roll and winding system. Both the single-screw extruder and the cast roll and winding system need to be set to the applicable parameters for the two parts to work together in coordination. The single-screw extruder is equipped with four heating zones and fed directly through a metal hopper. The granules are added to the single-screw extruder which gradually heats and melts the blend through four heating zones. The blend passed through the single-screw extruder enters the die. The blend is continuously heated to maintain a molten state. The molten composite flows from the lip of the die and enters the

cast roll and the winding system. The screw of the single-screw extruder is made of 38CrMoAl chrome-molybdenum alloy. The screw diameter is 20 mm and L/D is 25:1. The main components of the cast roll and winding system are the die, the cold roll, the rubber nip roll, and the take-up roll. The films with a thickness of 0.02–1.2 mm can be manufactured by adjusting the knob. One end of the knob is connected to the hydraulic control system and the other is connected to rubber nip roll. Rotating the knob can change the nip roller height to further control the thickness of the film. The chills roll is 200 mm OD and 320 mm wide. The rubber nip roll is 80 mm OD and 320 mm wide. The guide wheel is 30 mm OD and 320 mm wide. The winding roll is 80 mm OD and 320 mm wide, which uses friction to wind up films. As showed in Fig. 2, the die is a T-slot design. It consists of heating zone and connection zone. The heating zone has six zones. There are three small areas in the anterior part of the rectangular heating zone. The width of the die lip is 300 mm. The molten composite is extruded from the anterior three small areas (1, 2, 3 zones) and processed under the action of the pressure roller. There are also three small areas (4, 5, 6 zones) in the back part which are connected to the single-screw extruder outlet. The operating situation of the system are displayed on the processing condition monitor.

## Compounding and processing

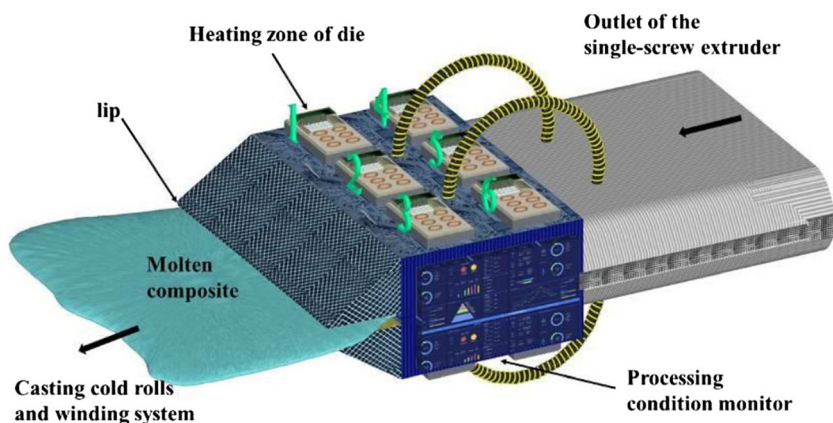
### Experimental system

As showed in Fig. 3 below, the experimental system of the development of high value-added new biomass composite wallpaper in this paper contains four parts, the development of nanoparticle-reinforced matrix (Part 1), the development of original composites (Part 2), the development of composites treated with solid dyes (Part 3), and the development of composites treated with liquid dyes (Part 4). The entire

**Table 3** Introduction of reagents and substances

| Label | Classification/function                        | Composition                                   |
|-------|--|---|
| A     | Biomass component                              | Agricultural waste powders                    |
| B     | Plastic component #1                           | RLDPE   |
| C     | Plastic component #2                           | RLLDPE  |
| D     | filler   | Ultrafine kaolin                              |
| E     | Nanoparticle-reinforced matrix (granules no.1) | RLDPE;RLLDPE;HLA-TiO <sub>2</sub>             |
| F     | Solid staining agent/nano-strengthenener       | HLA-TiO <sub>2</sub>                          |
| G     | Coupling agent                                 | Lauryl methacrylate(LMA)                      |
| H     | Multifunctional curing agent                   | Solid waste oil particles                     |
| I     | Dyeware  | Erioglucine disodium salt                     |
| J     | Dyeing solution                                | Lauryl methacrylate/erioglucine disodium salt |
| L     | Special solvent                                | Calcium gluconate                             |
| K     | Adhesive/lubricant                             | Purified waste oil                            |

Fig. 2 Structure drawing of the die of the casting film machine



experimental system adopts a pyramidal structure to screen out the optimal formula layer by layer. The front part provides the raw material for the latter part.

As showed in Tables 4, 5, and 6 in part 1, the total mass of the basic composition in each sample is constant at 500 g. The ratio of the RLDPE and RLLDPE is changed to carry out the experiment while the mass of other ingredients is controlled. The purpose of this part is to screen out the best formulation of RLDPE and RLLDPE, on which based the granules of an optimal nanoparticle-reinforced matrix (granules no. 1) are produced. In part 2, the total mass of the basic composition in each sample is constant at 500 g. The ratio of the AWP and calcium gluconate is changed to carry out the experiment while the mass of granules no.1 and other ingredients is controlled. Part 2 is to screen out the best formulation of AWP and calcium gluconate, which provides optimal original composites (granules no. 2) for part 3. In part 3, the mass of granules

no. 2 is controlled at 500 g, the weight of HLA-TiO<sub>2</sub> is changed to carry out the experiment. HLA-TiO<sub>2</sub> is additionally added reagent which is not included in 500 g. Part 3 is to screen out the optimal weight of HLA-TiO<sub>2</sub>, which provides the granules of optimal composites treated with solid dyes (granules no. 3) for part 4. In part 4, the mass of granules no. 3 is controlled at 515 g and the addition of the weight of the dyeing solvent is controlled at 30 g, while the concentration of dyeing solution is changed to carry out the experiment. Part 4 is to screen out the best dyeing solvent concentration, which is the basis for the development of colored scented biomass composite wallpaper.

**The raw material pretreatment section**

The moisture in the air enters AWP during transportation and storage, which causes agglomeration. As showed in Fig. 4

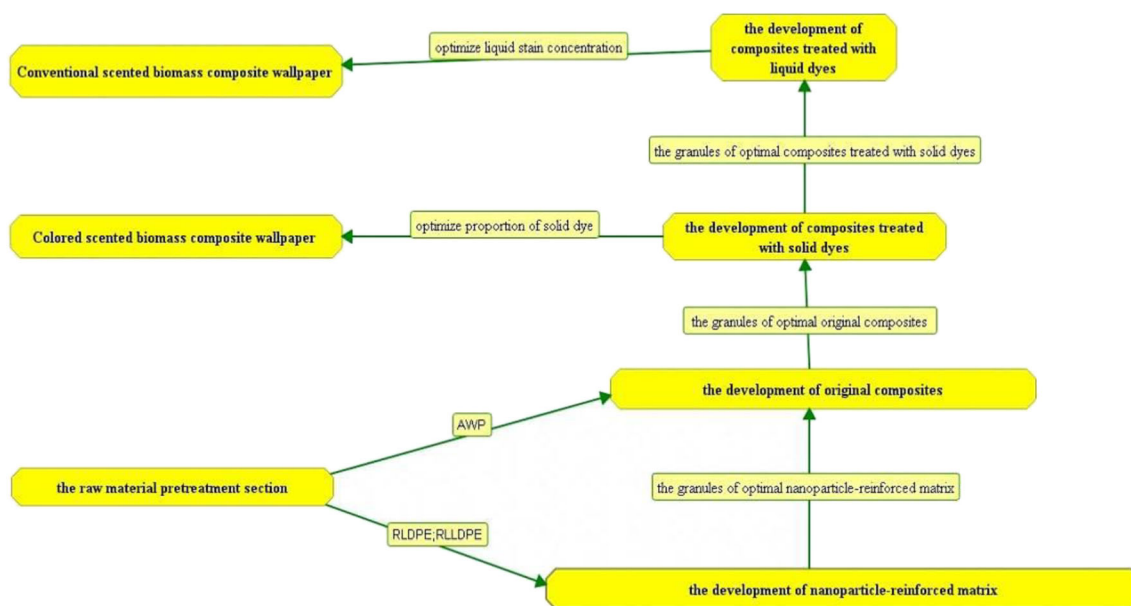


Fig. 3 The experimental system of the development of high value-added new biomass composite wallpaper

**Table 4** List of ingredients of the part 1

| Code | Part1<br>Composition                 | B:C    | The amount of various raw materials added |     |    |   |
|------|--------------------------------------|--------|---|-----|----|---|
|      |                                      |        | B   | C   | F  | K |
| 1    | BCFK (47/50/2/1)                     | 1:1.06 | 235                                       | 250 | 10 | 5 |
| 2    | BCFK (57/40/2/1)                     | 1:0.70 | 285                                       | 200 | 10 | 5 |
| 3    | BCFK (67/30/2/1)                     | 1:0.44 | 335                                       | 150 | 10 | 5 |
| 4    | BCFK (77/20/2/1) & E (granules no.1) | 1:0.26 | 385                                       | 100 | 10 | 5 |
| 5    | BCFK (87/10/2/1)                     | 1:0.11 | 435                                       | 50  | 10 | 5 |
| 6    | BCFK (92/5/2/1)                      | 1:0.05 | 460                                       | 25  | 10 | 5 |
| 7    | B (100)                              | Na     | 500                                       | 0   | 0  | 0 |
| 8    | BFK(97/2/1)                          | Na     | 485                                       | 0   | 10 | 5 |
| 9    | C(100)                               | Na     | 0   | 500 | 0  | 0 |
| 10   | CFK (97/2/1)                         | Na     | 0   | 485 | 10 | 5 |

above, a superfine pulverizer WFJ-60 (Zhengze, Jiangyin, China) and 500 mesh screens are used to process the agricultural waste powders. Refined straw powders are only optimized for particle size, they also carry a lot of dust and pesticide residues. The next step is to place deionized water in several 2-L beakers containing the AWP and place them on magnetic stirrers. Heat the water to 100 °C and mix the mixture evenly. The boiling process can promote the decomposition of impurities such as wax and pectin of biomass. Boiling water soaking treatment takes an hour, after which the suction filter bottles, funnels, and vacuum pumps (Secris, Henan, China) are used to separate. Then the separated AWP are placed in several 1-L evaporating dishes with covers. The separated AWP in the evaporating dishes are immersed with an appropriate amount of 8% sodium hydroxide. The evaporating dishes are placed in several KQ-500E ultrasonic generators (Chenglian, Shanghai, China) whose working temperature is set to 80 °C and working time is set to 2 h.

After the ultrasound-assisted lye soaking treatment, the AWP undergo a complete set of standardized washing, sterilization, and drying procedures finished by JP-2012GH automatic washing machine (Jiemeng, Shenzhen, China). The cavitation of the ultrasonic waves makes the plant fibers in the

AWP loose. It also increases the specific surface area of the fibers and promotes the outflow of impurities. The role of the lye is to increase the surface hydroxyl groups of AWP and activate the existing surface hydroxyl groups of AWP. Ding Fangfang (Fangfang et al. 2011) also used an approximate pretreatment method in the preparation of corn stalk fiber/PBS composites and had good results. The purified waste oil is taken from the refrigeration system. A ZNCL-BS smart magnetic stirrer (Yue Zhong, Shanghai, China) and 50-ml beakers are used to heat oil to 80 °C. This process can reduce the absolute viscosity of oil to 3.8–4.5 cP. The oil with better fluidity does not block the pipeline. The heated oil is poured into stainless steel sprayers (Maijia, Guangzhou, China). Some ash and salt enter plastic material during transportation and storage. The RLDPE and RLLDPE also are processed by the automatic washing machine. Stainless steel mesh boxes are used to carry the cleaned RLDPE and RLLDPE.

### Compounding process of composites

In many reports, the direct utilization of the ellipsoidal LDPE particles produced by the factory and extremely fine biomass powders causes some problems. The low relative specific

**Table 5** List of ingredients of the part 2

| Code          | Composition                           | A:L    | A   | D  | E   | H  | L   |
|---------------|---------------------------------------|--------|-----|----|-----|----|-----|
| 11            | ADE (granules no. 1) HL (0/3/75/2/20) | Na     | 0   | 15 | 375 | 10 | 100 |
| 12            | ADE (granules no. 1) HL (4/3/75/2/16) | 1:4    | 20  | 15 | 375 | 10 | 80  |
| 13            | ADE (granules no. 1) HL (8/3/75/2/12) | 1:1.5  | 40  | 15 | 375 | 10 | 60  |
| 14            | ADE (granules no. 1) HL(10/3/75/2/10) | 1:1    | 50  | 15 | 375 | 10 | 50  |
| 15            | ADE (granules no. 1) HL (12/3/75/2/8) | 1:0.67 | 60  | 15 | 375 | 10 | 40  |
| 16            | ADE (granules no. 1) HL (16/3/75/2/4) | 1:0.25 | 80  | 15 | 375 | 10 | 20  |
| 17            | ADE (granules no. 1) HL (20/3/75/2/0) | Na     | 100 | 15 | 375 | 10 | 0   |
| Granules no.2 | ADE (granules no. 1) HL (8/3/75/2/12) | 1:1.5  | 40  | 15 | 375 | 10 | 60  |

**Table 6** Lists of ingredients of the part 3 and part 4

| Code           | Composition       | Ganules no. 2 | F   | Code                             | Composition; additive amount of dye solvent | Ganules no. 3 | I   | J  | $\beta$ (%) |
|----------------|-------------------|---------------|-----|----------------------------------|---|---------------|-----|----|-------------|
| 18             | Granules no. 2; F | 500           | 2.5 | 24                               | Granules no. 3 (515 g); J (30 g)            | 515           | 0   | 50 | 0           |
| 19             | Granules no. 2; F | 500           | 5   | 25                               | Granules no. 3 (515 g); J (30 g)            | 515           | 0.2 | 50 | 0.40        |
| 20             | Granules no. 2; F | 500           | 10  | 26                               | Granules no. 3 (515 g); J (30 g)            | 515           | 0.5 | 50 | 0.99        |
| 21             | Granules no. 2; F | 500           | 15  | 27                               | Granules no. 3 (515 g); J (30 g)            | 515           | 1   | 50 | 1.96        |
| 22             | Granules no. 2; F | 500           | 20  | 28                               | Granules no. 3 (515 g); J (30 g)            | 515           | 1.5 | 50 | 2.91        |
| 23             | Granules no. 2; F | 500           | 25  | 29                               | Granules no. 3 (515 g); J (30 g)            | 515           | 2   | 50 | 3.85        |
| Granules no. 3 | Granules no. 2; F | 500           | 15  | Concentration: $\beta = I/J(\%)$ |   |               |     |    |             |

surface area of the ellipsoidal LDPE particles will lead to uneven mixing of filler and plastic. The low relative specific surface area also let fillers not completely penetrate into the matrix. The extremely fine biomass powders require more advanced grinding techniques which cause the cost to rise sharply, while static electricity increases agglomeration of powders. In part 1, innovative screw wire pulling granulation technology and particle surface coating liquid film technology are used to solve these problems. The parameters of the twin-screw extruder required for the wire pulling granulation technology are as shown in Table 7 and Fig. 5. The weights of ingredients are weighed with a YP1002 electronic balance (Dingke, Shanghai, China).

This linear temperature profile causes the ellipsoidal plastic particles to be gradually heated to a temperature of about 170 °C above their melting point and the molten plastic has good deformation and ductility. As showed in Fig. 5, the intelligent pelletizer uses a gear-shaped blade to bite the wire and the shaft torque can be changed to apply a larger axial pulling force to the wires by increasing the speed. The axial friction generated by the conveyor belt which directly contacted with the wire. The molten plastic is subjected to not only the axial pulling action of the pelletizer and the conveyor belt but also the radial pressing action of the twin-screw extruder. Under the combined action, the molten plastic becomes ultra-fine plastic wires which are cut into small cylindrical plastic particles by the blade of the pelletizer. The small cylindrical RLDPE granules are produced. The particle surface coating liquid film technology facilitates better contact between the HLA-TiO<sub>2</sub> powders and the plastic granules. Several stainless steel sprayers (Maijia, Guangzhou, China) containing heated purified waste oil are used to spray the oil mist onto the surface of the plastic particles. The oil covers the surface of the oval plastic particles to form an oil film. The respective weights of the oil and plastic particles are weighed with balance before this process. After spraying 2–3 times at different angles using a sprayer, the stainless steel spoon was used to stir the mixture. Repeat this operation several times until the oil is consumed. Then HLA-TiO<sub>2</sub> powders are added to the pot using a small spoon and the mixture is stirred with the stainless steel spoon. The amount of HLA-TiO<sub>2</sub> powders

added in one time is 1–2 g and the addition is completed in 3–4 times. This operation allows the HLA-TiO<sub>2</sub> powders to be uniformly adhered to the surface of plastic granules which coated with a uniform oil film. In addition to strengthening of the properties of the composite, the white HLA-TiO<sub>2</sub> nanoparticles play a role as a marker to distinguish composite from the ordinary RLDPE wires. Finally, the mixture is sent to a twin-screw extruder for compounding processing according to the following parameter settings. Purified waste oil not only functions as an adhesive but also acts as a lubricant to promote better movement of the molten material under the action of the two screws (Table 8).

As shown in Tables 4, 5, and 6, the twin-screw compounding process in part 1 produced a total of ten kinds of granules. They are fed to a cast film machine under the parameters shown in Table 10 to produce corresponding film samples. The optimal ratio of RLDPE and RLLDPE is selected according to the mechanical analysis of these samples, on which based a large number of granules no. 1 for part 2 are produced. As shown in Table 9, a small cylindrical granule no. 1 has a specific surface area of 3.889 mm<sup>2</sup>/mm<sup>3</sup>, which is about twice the specific surface area of an ellipsoidal normal plastic granule. The small cylindrical RLDPE granule has the highest specific surface area of 4.567 mm<sup>2</sup>/mm<sup>3</sup>. These two technologies result in an increase in the contact area of the matrix with the fillers and allow the fillers to be better embedded into the matrix Fig. 6.

As shown in Table 11, granules no. 1 in part 2 and other ingredients are premixed by pots, spoons, and YLT-50L small experimental high-efficiency mixer (Yilang, Guangdong, China). The high-efficiency mixer has a temperature range between 30 and 150 °C, a speed adjustment between 0 and 50 rpm, and a pneumatic discharge mode. Steps 1 to 2 are used to dehumidify. Steps 3 to 7 are used to gradually mix the various starting materials to obtain a homogeneous mixture.

The mixture processed by the YLT-50L small experimental high-efficiency mixer is poured into a twin-screw extruder and subjected to a compounding process under the parameters showed in the following Table 12. The granules are fed to a cast film machine under the parameters shown in the above Table 10 to produce the samples.

**Fig. 4** The processing system of the development of high value-added new biomass composite wallpaper



Granules no. 2 for part 3 are obtained by the same analysis and selection method as granules no. 1.

**Table 7** The parameters of the twin-screw extruder required for production of the small RLDPE cylindrical plastic particles

| Zone number | 6(die) | 5   | 4   | 3   | 2   | 1   | S <sub>1</sub> | S <sub>2</sub> | S <sub>3</sub> | S <sub>4</sub> | P <sub>1</sub> |     |
|-------------|--------|-----|-----|-----|-----|-----|----------------|----------------|----------------|----------------|----------------|-----|
|             | °C ± 5 |     |     |     |     |     | r/min          |                |                |                |                | bar |
| Temperature | 190    | 180 | 160 | 140 | 120 | 100 | 6              | 8              | 5              | 49             | 3–7            |     |

S<sub>1</sub> feed screw speed, S<sub>2</sub> twin screw speed, S<sub>3</sub> conveyor speed, S<sub>4</sub> pelletizer cutting speed, P<sub>1</sub> Twin screw internal pressure

Granules no. 2 from part 2 above are baked in the HLB-965 electronic plastic baking box (Hualu, Dongwan, China) at 140 °C for 1 h. The baking process not only removes moisture but also melts the mixture of glucose and biomass on the surface of the granules (Table 11). This process makes the HLA-TiO<sub>2</sub> powders to stick to the surface of the granules. The baked granules and HLA-TiO<sub>2</sub> powders are mixed in a pot using a big spoon. The amount of HLA-TiO<sub>2</sub> powder added in one time is 1–2 g and the addition is completed in several times. HLA-TiO<sub>2</sub> powder-coated granules are



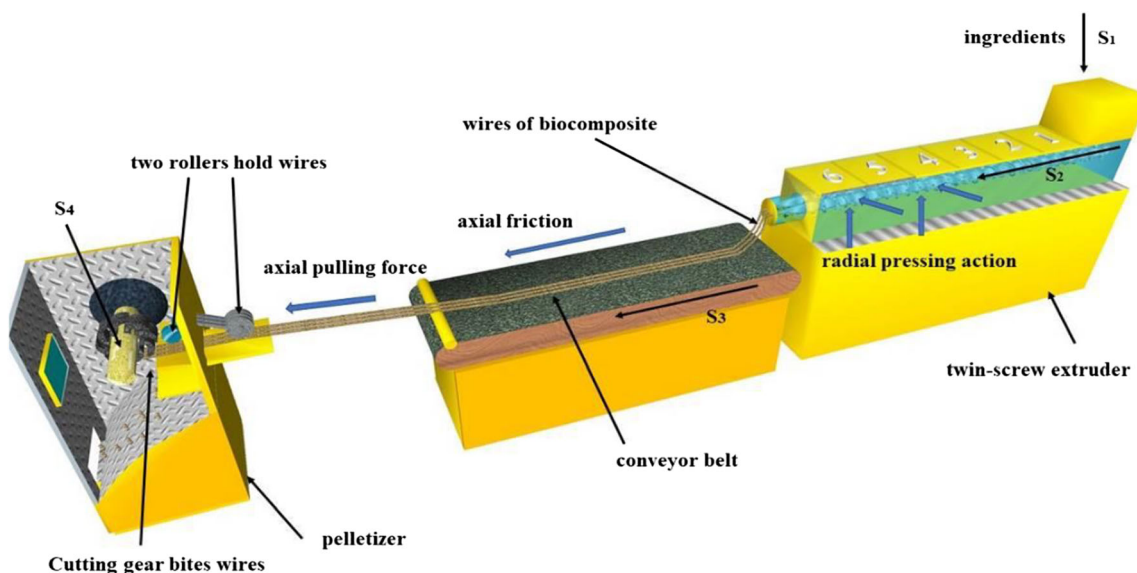


Fig. 5 Working principle diagram of twin-screw extruder

subjected to a compounding process under the parameters showed in Table 12. Granules no. 3 for part 4 are selected and obtained by the same method above.

In part 4, the lauryl methacrylate from the refrigeration system is poured into a 50-ml small beaker and a stirrer is used to heat it to 80 °C which makes the solvent have better fluidity. After setting the ZNCL-BS smart magnetic stirrer’s speed to 10 rpm, the erioglaucine disodium salt was added to the solution with a small spoon. The amount of solute added in one time is 0.1–0.2 g and the addition is completed in several times. The obtained dye solution is poured into several stainless steel sprayers which are used to spray the dye solution mist onto the surface of granules no. 3. After spraying two to three times at different angles using a sprayer, the stainless steel spoon was used to stir the mixture. The dyed granules are fed to a twin-screw extruder and a cast film machine under the parameters which are the same as the parameters in part 2. The best formula can be obtained by the research of granules no. 3 treated with different concentrations of dye solution, which is used to produce products.

### Measurement and analysis

#### Mechanical analysis

The LX-DN-LL101 type 10 kN electronic universal testing machine (Lixiong, Dongwan, China) is used to determine the mechanical properties of the biocomposite sheets based on ISO 527-1: 1993 and ISO 527-3: 1995, whose precision of force measurement is 0.5%. The manufactured biocomposite sheets were processed into the specified sample (sample type 2 illustrated by the above specification) at 200 mm long and 10 mm wide by 5410801 type photo cutting machine (Fellowes, Shanghai, China) according to the ISO standard. The electronic universal testing machine has a programmable operator panel that can be used to program special formulas. The Young’s modulus is obtained by importing the machine with the following formula by referring to the standard ISO 527-1: 1993. The test speed is 50 mm/min, and the speed measurement accuracy is 0.5%.

$$E_t = \frac{\sigma_2 - \sigma_1}{\varepsilon_2 - \varepsilon_1}$$

$E_t$ : elastic modulus (Mpa);

$\sigma_2$ : the measure stress value when the strain value  $\varepsilon_2$  is 0.0005;

$\sigma_1$ : the measured stress value when the strain value  $\varepsilon_2$  is 0.0025

Eight test strips were used for each sample measurement. The average of the test data represents the mechanical properties of the sample. The distance between the two fixtures is 100 mm ( $\pm 5$  mm). An external extensometer with a 50-mm grip separating distance is used. Each sample’s width was

Table 8 The parameters of the twin-screw extruder required for the development of nanoparticle-reinforced matrix

| Zone number | 6(die) | 5          | 4   | 3   | 2   | 1  | S <sub>1</sub> | S <sub>2</sub> | S <sub>3</sub> | S <sub>4</sub> | P <sub>1</sub> |
|-------------|--------|------------|-----|-----|-----|----|----------------|----------------|----------------|----------------|----------------|
|             |        | °C $\pm 5$ |     |     |     |    | r/min          |                |                |                | bar            |
| Temperature | 180    | 160        | 140 | 120 | 100 | 80 | 7              | 9              | 5              | 49             | 4–8            |

**Table 9** The parameters of three types granules

| Granules type                       | Particle size (mm)               | Calculation formula   | Specific surface area ( $S_V$ )  |
|-------------------------------------|----------------------------------|---|----------------------------------|
| Small cylindrical granules No.1     | 1.2 & 3.6 ( $d_1$ & $h_1$ )      | $S_V = \left( \frac{\pi d_1^2}{2} + \pi d_1 h_1 \right) / \left( \frac{\pi d_1^2}{4} h_1 \right)$ | $3.889 \text{ mm}^2/\text{mm}^3$ |
| Small cylindrical RLDPE granules    | 1 & 3.5 ( $d_2$ & $h_2$ )        | $S_V = \left( \frac{\pi d_2^2}{2} + \pi d_2 h_2 \right) / \left( \frac{\pi d_2^2}{4} h_2 \right)$ | $4.567 \text{ mm}^2/\text{mm}^3$ |
| Ellipsoidal normal plastic granules | 3 & 2 & 2 ( $2a$ & $2b$ & $2c$ ) | $S_V = \left[ \frac{4}{3} \pi (ab + bc + ca) \right] / \left( \frac{4}{3} \pi abc \right)$        | $1.778 \text{ mm}^2/\text{mm}^3$ |

measured with a Vernier caliper (accuracy = 0.02 mm) and its thickness was measured with a micrometer (accuracy = 0.001 mm). Three measurement points, 40 mm apart, are taken on each sample to estimate the average thickness of each sample. The average sample thickness was calculated and the cross-sectional area was calculated.

### Micromorphology observation

The samples were subjected to liquid nitrogen freezing treatment and a good surface was obtained before the micromorphology observation. Before the micromorphology observation, the samples are bonded to observation bases by conductive glue. The colored images of the samples without metal spraying process are taken firstly by the AxioVision\_SE641\_SP2 3D microscope (ZEISS, USA). This microscope is equipped with Z-axis series shooting technology and Nyquist graphics optimization algorithm. The details and features of the particularly rough surface of the samples which are sputter-coated with gold are observed by JSM-7610F field emission scanning electronic microscope (HITACHI, Japan) and Tungsten gun emission scanning electron microscope (FEI, Czech Republic).

### The Chroma detection

The Chroma detection of the processed colored scented biomass composite wallpaper is finished by YS6060 desktop

grating spectrophotometer (3Nh, Shenzhen, China), whose illumination mode: reflection D/8°, transmission D/0° (including UV/exclude UV measurement). YS6060 desktop grating spectrophotometer also has a TFT true color 7 in. capacitive touch screen, a full light source, and a dual array 256-pixel CMOS detector. After black and white correction, the total color difference can be obtained by using this device. The color card of the sample can be obtained by inputting the lab value of the sample into a color converter. The calculation formula of the total color difference value is designed according to the equipment specification and the relevant standard (ISO 11664-4:2008).

$$\Delta E = \left[ (L_0 - L)^2 + (a_0 - a)^2 + (b_0 - b)^2 \right]^{1/2}$$

$L_0, a_0, b_0$ :  $L, a, b$  values of white base as standard

$L, a, b$ :  $L, a, b$  values of the sample

$\Delta E$ : total color difference

When using a white base as standard, the formula changes to the following form:

$$\Delta E = \left[ (100 - L)^2 + a^2 + b^2 \right]^{1/2}$$

In order to better observe the color, detail, and flaws of the object, a EOS-1DX Mark II digital SLR camera (Canon, Japan) is used to take photos of the sample. The body of this camera is made of magnesium alloy, with effective pixels of



**Fig. 6** Physical photos small cylindrical RLDPE granules, small cylindrical granules no. 1, and ellipsoidal normal plastic granules

**Table 10** The parameters of the cast film machine

| 1. Single screw extruder parameters                     |                |        |        |                   |                    |           |
|---|----------------|--------|--------|-------------------|--------------------|-----------|
| Zone number   | 4 (die)        | 3      | 2      | 1                 | $S_5$              | $P_2$     |
|   | 175 °C         | 150 °C | 125 °C | 100 °C            | 60 rpm             | 19–23 bar |
| 2. The casting chill roll and winding system parameters |                |        |        |                   |                    |           |
| Die zone position                                       | Temperature °C |        |        | Winding speed rpm | Traction speed rpm |           |
| Exit  | 175(1)         | 175(2) | 175(3) | 152               |                    |           |
| Entrance  | 175(4)         | 160(5) | 175(6) |                   | 88                 |           |

$S_5$  screw speed,  $P_2$  internal pressure of the single screw extruder

2020 megapixels, sensor type CMOS, ISO sensitivity of ISO 100-51200.

## Results and discussions

### Liquefaction filling technology and hybrid network model construction technology

Based on the results of the various measurements above, the mechanism of the material formation process can be analyzed. Based on this mechanism, the theory of the liquefaction filling technology and hybrid network model (Table 13) construction technology can be developed. As showed in Fig. 7, state 1 is the microstructure of the nanoparticle-reinforced matrix, which shows that the HLA-TiO<sub>2</sub> nanoparticles coated with purified waste oil are uniformly dispersed in the hybrid plastic matrix of RLDPE and RLLDPE. The uniform dispersion of the nanoparticles has a reinforcing effect on the material properties. The nanoparticle-reinforced matrix can be used as a basic material for the development of other kinds of materials. State 2 illustrates the formation mechanism of the original composites. To make the illustration clearer, it is divided into state 2.1 and state 2.2. State 2.1 shows the initial composite state of the raw material entering the twin-screw extruder. State 2.2 shows the microstructure of the granules of the

original composites. As showed in state 2.1, the particles of AWP, calcium gluconate, and ultrafine kaolin are mixed into the nanoparticle-reinforced matrix and their distribution is messy. The particles of AWP and calcium gluconate are in contact with each other and are uniformly mixed. Solid waste oil particles are rapidly heated and melted. They distribute in the form of thin strips inside the material to act as a lubricant. The ordinary liquid solvent like water will stick the powder into blocks, which cause blockage of the channel, but the calcium gluconate does not have this problem as a special solvent. As showed in state 2.2, the ingredients in the twin-screw extruder are in a high-temperature and high-pressure environment. They are also subjected to shear forces applied by the screw. The solid solvent calcium gluconate becomes liquid. The liquid calcium gluconate is uniformly mixed with AWP in the form of fine powders to form a solvent. Both cellulose and calcium gluconate are sugars. Both AWP and calcium gluconate contain a large number of hydroxyl groups and have a certain structural similarity, which makes them have good affinity and compatibility with each other. Hybrids of AWP and calcium gluconate based on the theory of similarity and intermiscibility are uniformly diffused in the form of a liquid in the nanoparticle-reinforced matrix. The hybrids are subjected to shear forces from the screw, tension from the pelletizer, and pressure from the liquid plastic and cavity. The hybrids are dispersed in the material in an irregular sheet form. Most of AWP and calcium gluconate are mixed with each other to form a solution, which is mixed into the nano-matrix as a kind of liquid biomass filler. A kind of new hybrid is formed by mixing the liquid biomass filler with a portion of the liquid plastic, which exhibits an irregular sheet-like structure after cooling and solidification. Some of AWP and calcium gluconate fuse with each other. They form another kind of hybrid of a neuron-like structure embedded in the sheet structure due to unavoidable agglomeration and local differences. This neuron-like structure is mainly composed of the composite of biomass, glucose, and liquid plastic. It also contains a small number of biomass particles. It can be attached to the sheet-like structure with less impact on the properties of the material. Unlike the traditional filling

**Table 11** The corresponding method of adding and mixing raw materials

| Step | Substance     | Equipment           | Temperature and time |
|------|---------------|---------------------|----------------------|
| 1    | A, E          | Pots and spoons     | 22 °C & 2 min        |
| 2    | A, E          | High mixing machine | 100 °C & 10 min      |
| 3    | A, E, L       | Pots and spoons     | 22 °C & 2 min        |
| 4    | A, E, L       | High mixing machine | 60 °C & 3 min        |
| 5    | A, E, L,D     | Pots and spoons     | 22 °C & 2 min        |
| 6    | A, E, L,D     | High mixing machine | 60 °C & 3 min        |
| 7    | A, D, E, L, H | Pots and spoons     | 22 °C & 3 min        |

**Table 12** The parameters of the twin-screw extruder required in part 2

| Zone number | 6 (die)<br>°C ± 5 | 5   | 4   | 3   | 2   | 1   | S <sub>1</sub><br>r/min | S <sub>2</sub> | S <sub>3</sub> | S <sub>4</sub> | P <sub>1</sub><br>bar |
|-------------|-------------------|-----|-----|-----|-----|-----|-------------------------|----------------|----------------|----------------|-----------------------|
| Temperature | 175               | 180 | 175 | 150 | 120 | 100 | 15                      | 35             | 5              | 15             | 18–22 bar             |

technology, the biomass component is mixed with liquid plastic in liquid form and has a good dispersibility. The special sheet-like structures produced by this technology not only has a large contact area with the plastic matrix but also form the framework with the matrix. The purpose of ultrafine kaolin is to fill a small number of inevitable voids inside the material. State 3 illustrates the microstructure of the composites treated with solid dyes. After repeated compound processing, the sheet-like structures change greatly. Some of the sheet-like structures become longer and thinner under the combined action, showing a long strip shape. The other sheet-like structures are split. The splitted structures are adhered to the long strip shape structure to form several kelp-like branch structures. This new long strip shape structures with kelp-like branch structures are the grown sheet-like structures. In addition to some changes in appearance, the new structures have denser structures than the sheet-like structure of the previous state 2 due to the more complete fusion. As the fusion process is more complete, the neuron-like structures have undergone some changes. Their tentacles become longer and they themselves become longer and thinner. The appearance of the grown sheet-like structures and the grown neuron-like structures is due to the more complete fusion process and the long-term synergy of the three mechanical effects. A lot of HLA-TiO<sub>2</sub> nanoparticles are attached to their dense structure. In addition to changing the overall color, nanoparticles increase the overall stiffness of the material. State 4 illustrates the microstructure of the composites treated with liquid dyes. The feature of this microstructure is the presence of a large number

of network structures. There are two types of network-like structures. The first type is like a fine fishing net which is produced by the polymerization and cross-linking reaction of lauryl methacrylate itself. The second type is like a neural network in the human body. The lauryl methacrylate fused with the grown neuron-like structure of state 3 undergoes polymerization and cross-linking reaction, thereby connecting the grown neuron-like structures to each other to form a network. The first type is directly embedded in the grown sheet-like structure, while the second type is overlaid on the first layer and entangled with the first network. This composite network structure not only has good elasticity but also fills in tiny cracks in the material.

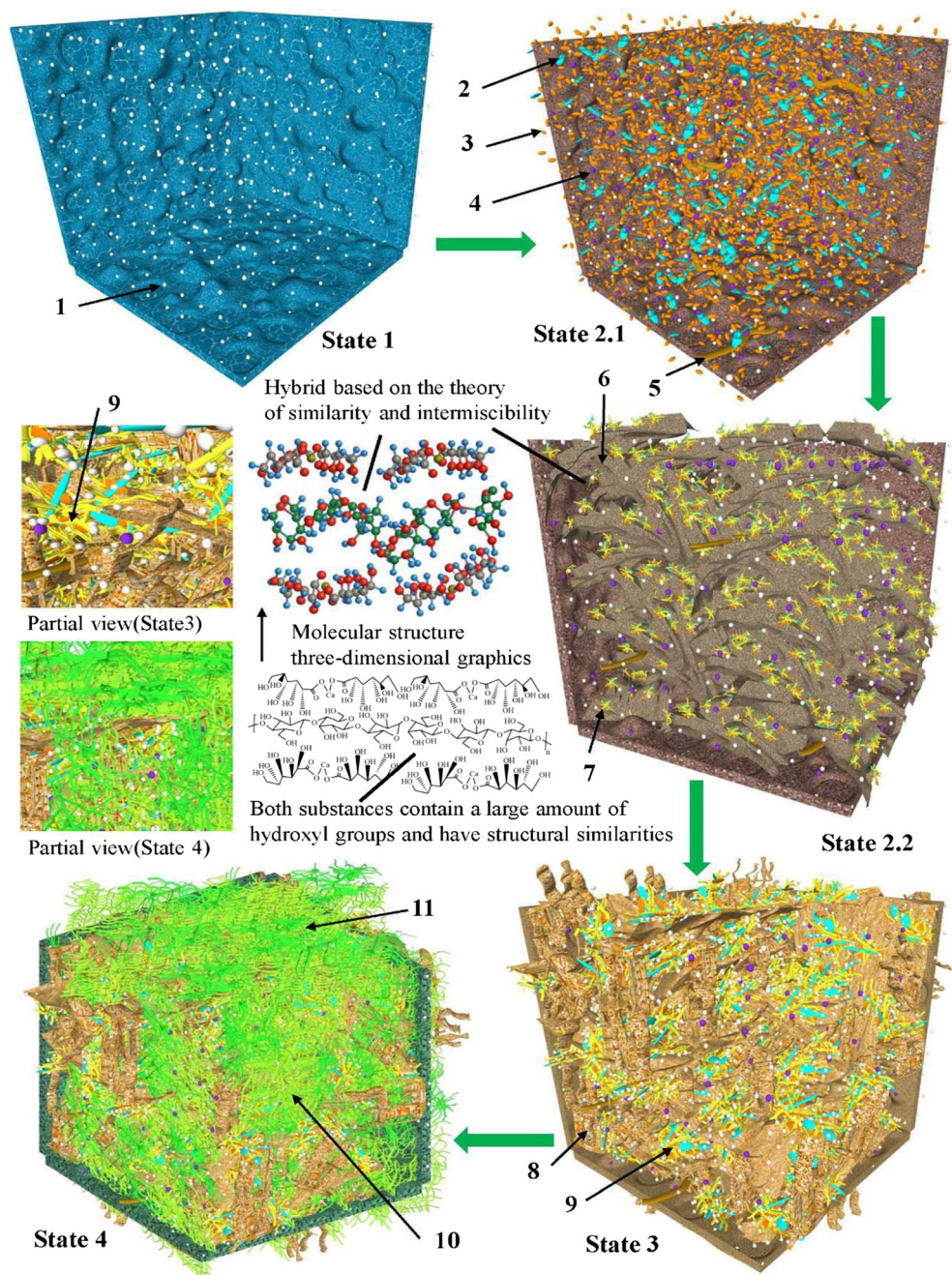
### Mechanical properties of material

The high value-added new scented biomass composite wallpaper is produced by the casting film machine. Tensile strength(TS), elongation at break(EAB), and Young's modulus (YM) are three important indicators for assessing their mechanical properties. Figure 8 shows the effect of nanoparticle content on the mechanical properties of matrix reinforced by nanoparticles. Comparison of sample 7 and sample 8 found that the TS of the material increased from 14.5 to 16.1 MP. Comparison of sample 9 and sample 10 found that the TS of the material increased from 6.1 to 7.3 MP. The addition of 2 wt% HLA-TiO<sub>2</sub> can increase the TS, EAB, and YM of the material. Researcher Laida (Cano et al. 2017) also obtained similar conclusions when studying the effect of nano titanium

**Table 13** Supplementary description of the schematic diagram

| Code | Name                                | Color  |
|------|-------------------------------------|--|
| 1    | HLA-TiO <sub>2</sub> nanoparticles  | Pure white                                   |
| 2    | Calcium gluconate                   | Light blue                                   |
| 3    | AWP particles                       | Orange                                       |
| 4    | Ultrafine kaolin particles          | Purple                                       |
| 5    | Molten solid waste oil particles    | Dark yellow                                  |
| 6    | The sheet-like structure            | Brown  |
| 7    | The neuron-like structure           | Golden(fused structure); orange; light blue  |
| 8    | The grown sheet-like structure      | Wheat-colored                                |
| 9    | The grown neuron-like structure     | Golden (fused structure); orange; light blue |
| 10   | First type network-like structures  | Light green                                  |
| 11   | Second type network-like structures | Dark green                                   |

**Fig. 7** The schematic diagram of the entire microscopic mechanism of the material formation process



dioxide on the properties of nanocomposites. LDPE has long chain branches, while LLDPE has only short chain branches. This makes RLLDPE more rigid than RLDPE, which means RLLDPE has a higher YM. It also explains that the YM of samples 1 to 6 drops from 673.7 to 259.2 MPa. The addition of nanoparticles also increases the YM of the material due to the relatively high hardness of the nanoparticles themselves. Both RLLDPE and RLDPE are recycled and reprocessed plastics, and their mechanical properties deteriorate and change a lot compared to new plastics. The lower the grade of waste plastic, the worse the mechanical properties of recycled plastics. Adding nanoparticles to RLLDPE not only

improves the overall stiffness of the composite but also transfers stress (Nagarajan et al. 2013). As shown in Figs. 11 and 12, the comparison of the micrographs of sample no. 13 and sample no. 18 found that after adding some nanoparticles, the gap in the sample not only decreased in size but also decreased in depth. SEM pictures of the two samples indicate that gaps in the sample not only changed in size but also changed in shape. The nanoparticles fill many small gaps existing in the RLLDPE and the stress is transmitted uniformly and effectively when the material is subjected to a tensile force applied by the universal testing machine. This is beneficial to the plastic deformation of the material and prevents the partial tear of the

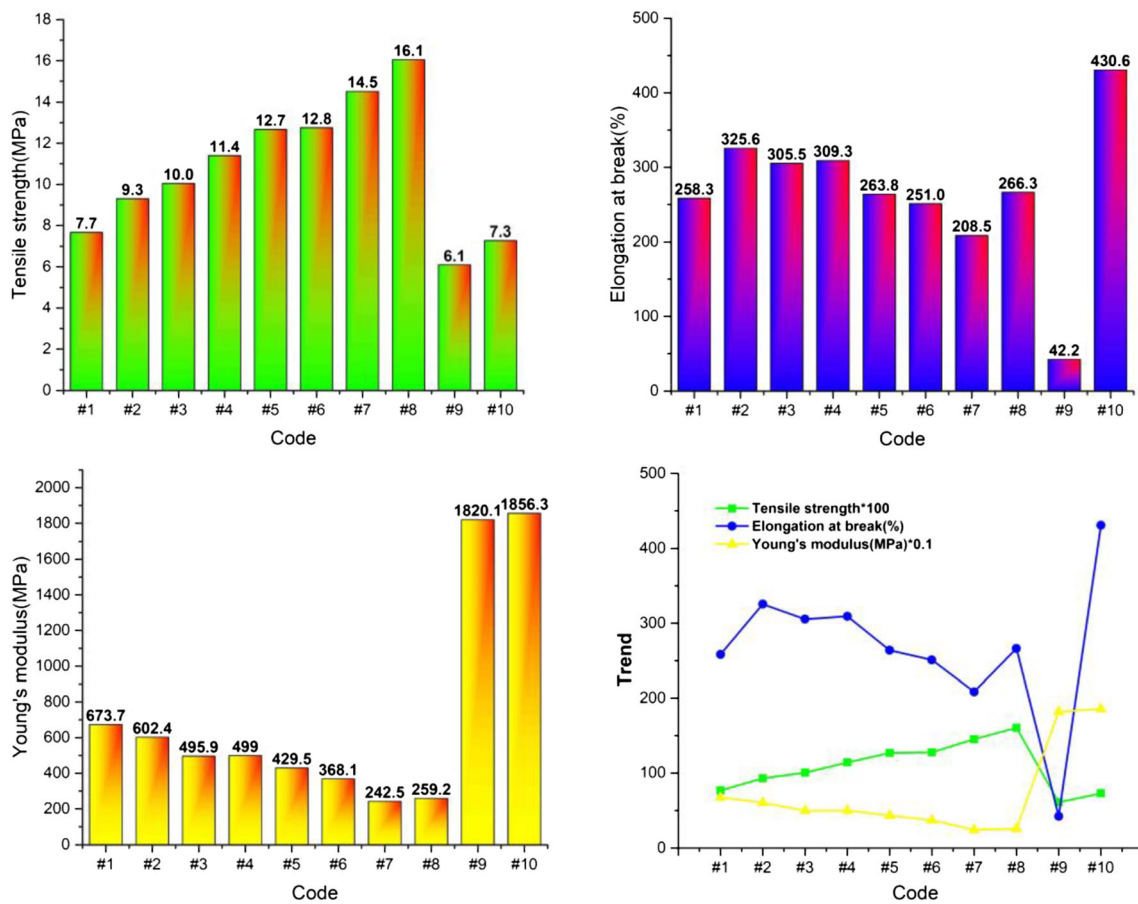


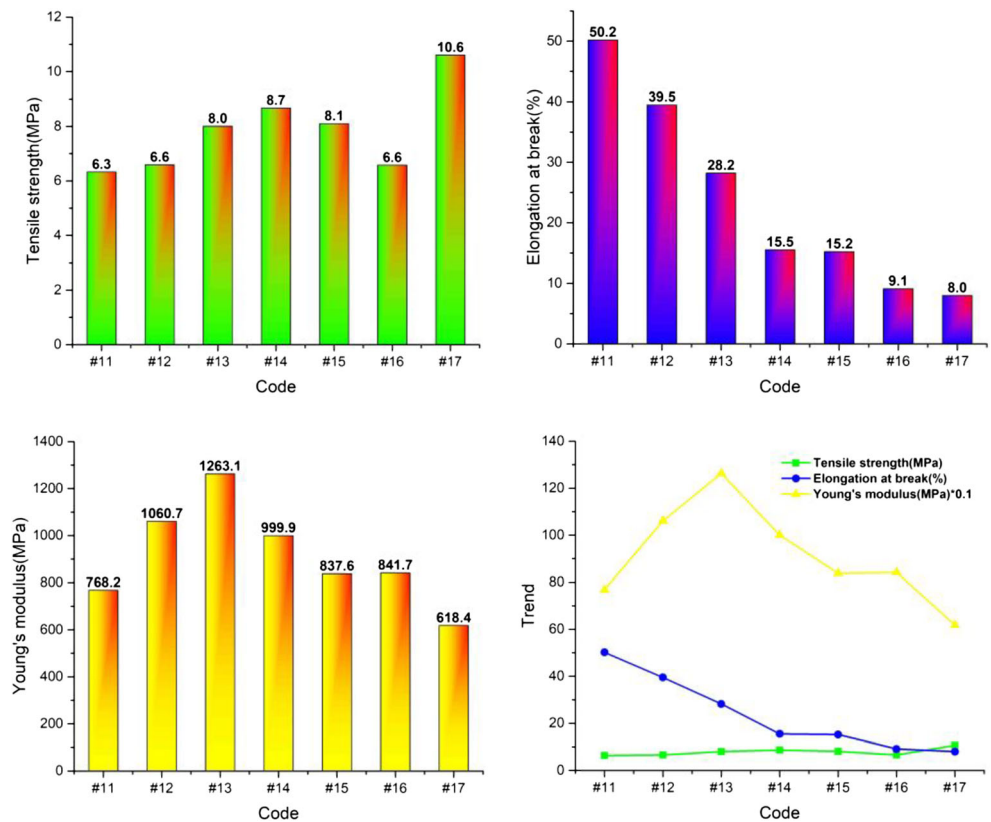
**Fig. 8** Columnar section drawing of mechanical properties of sample 1 to sample 10

material. RLLDPE has a high EAB because of its molecular structure characterized by linear backbones. As a kind of third-class recycled plastic recycled from the plastic used twice and more than twice, RLLDPE has many impurity particles distributed unevenly inside, which makes it high in rigidity and high in YM. However, uneven impurity particles and gaps also cause many stress concentration points to reduce the TS of the material. The combination of RLLDPE and RLDPE can improve the overall deformability of the material while keeping the proper TS of the material. The addition amount of RLLDPE also has a certain regular relationship with the EAB. But when the ratio of RLLDPE and RLDPE is unreasonable, many fine cracks and gaps appear inside the material, which makes the partial tear is prone to occur and the TS of the material decrease. A suitable ratio allows the RLDPE and RLLDPE to be mixed more uniformly and the nanoparticles can better fill the cracks and transfer stress. As a kind of matrix material, the nanoparticle-reinforced matrix is required to have not only excellent ductility but also reasonable toughness and rigidity. Sample 4 has a relatively good EAB (309.3%), a suitable YM (499 MPa), and a suitable TS (11.4 MPa). Sample 4 not only meets the mechanical properties but also reduces the cost by containing a certain amount of

RLLDPE. As a result, it is the best nanoparticle-reinforced matrix for the development of original composites.

As shown in Fig. 9, samples 11 and 17 represent two specific composite materials, respectively. The biomass filler of sample 17 was embedded in the plastic matrix in the form of solid particles during the compounding process while the AWP of the sample 11 was uniformly mixed with the plastic matrix in a molten liquid state during the compounding process. The stress transfer of the particles gives sample 17 better TS (10.6 MPa). But granular biomass filler can destruct the structural integrity of the matrix (Njoku et al. 2012), which contributes to the low EAB values of the composites (8%). The addition of biomass particles with a certain hardness can increase the YM of the composite (Bhagat et al. 2014). However, the structure of ordinary biomass particles embedded in a plastic matrix is prone to local tensile fracture and deformation, which is not suitable for the development of wallpaper. In addition to cellulose, biomass particles also contain impurities such as hemicellulose, lignin, and pectin, which reduce the adhesion between the biomass particles and the hydrophobic plastic matrix (Ku et al. 2011). The composites in the twin-screw extruder are not only in high temperature and high pressure environment but also subjected to

**Fig. 9** Columnar section drawing of mechanical properties of sample 11 to sample 17



shear forces applied by the screw. The substances containing a large number of hydroxyl groups such as cellulose, hemicellulose, lignin, and pectin are dissolved in the liquid glucose containing hydroxyl groups based on the theory of similarity and intermiscibility. From sample 11 to sample 16, the biomass content of the composite gradually increased, but the TS of the composite increased from 6.3 to 8.7 MPa and then decreased to 6.6 MPa. The peak-like change in TS is similar to the discovery of Zhenghao Ge’s research of straw flour/styrene butadiene styrene composite (Ge et al. 2017). The change of YM also shows a peak shape, which first rises from 768.22 to 1263.1 MPa, then decreases to 841.7 MPa. The EAB has a different trend, it gradually decreased from 50.2 to 9.1% as the biomass content increased. The change in mechanical properties is mainly affected by the solubility of biomass components in liquid glucose. The liquid glucose of sample 11 is dispersed in the plastic, the damage to the substrate is small, so the composite has a high EAB. The YM of the original composite is increased compared to sample 4. The mobility of the plastic molecular chain in the composite formed by the addition of biomass is greatly limited, which causes the YM of the composite to rise. For sample 12, the concentration of biomass in glucose was relatively low and the solubility of biomass in glucose did not reach saturation. At this time, the overall performance of the composite has been slightly improved. For sample 15 and sample 16, the biomass component at this time was severely excessive, far exceeding

the solubility of glucose. Granular biomass fillers are present in large quantities. The interaction between the biomass fillers and the matrix is much weaker than the interaction between the biomass fillers, resulting in a decrease in the TS of the material. Some scholars have found similar phenomena in their research (Sreekumar et al. 2007) (Lowa et al. 2017). Agglomeration of particles creates several weak spots within the material sensitive to fracture, which damages the ductility of the material. For samples 13 and 14, the solubility of biomass in glucose is within a short interval around the saturation point. The solution of biomass and glucose in sample 13 is in an optimal state, when glucose dissolves most of the biomass particles and also contains traces of particles. This solution allows the filler to be uniformly dispersed in the molten state of the plastic, resulting in a large amount of chain interlacing inside the composite and good mechanical continuity of the system. The trace amount of particles increases the overall stiffness. The above reasons cause the YM of sample 13 to be the highest (1263.1 MPa). The biomass filler and glucose are dispersed in a plastic matrix in the form of a wide and irregularly shaped long piece structure which has a large contact area with the plastic matrix and a better compatibility. The long piece structure is very different from the hard particles. Hard particles can only cause serious obstacles to the molecular motion of the polymer chain (Guo et al. 2018). In addition to hindering the molecular motion of the polymer chain, long piece structure can transmit stress and have a certain degree of

plastic deformation under a certain degree of external tension. Among these samples, sample 13 has the best comprehensive mechanical properties (TS 8.0 MPa; EAB 28.2%; YM 1263.1 Mpa).

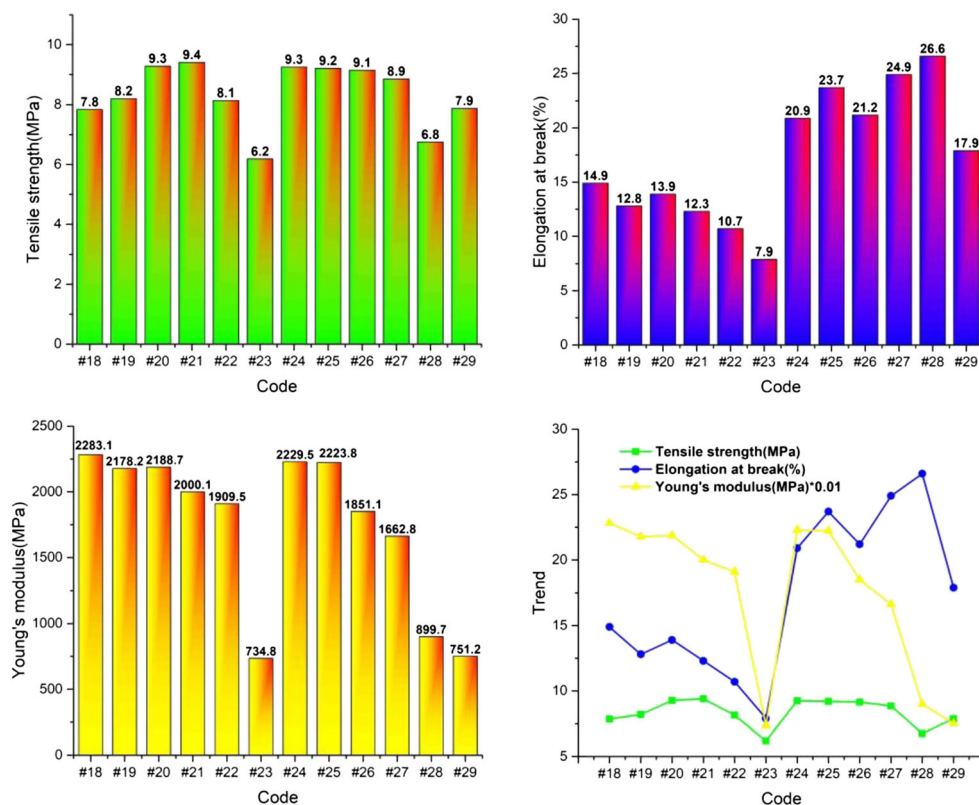
The addition of HLA-TiO<sub>2</sub> has two effects on the material, which affects the mechanical properties of the material in addition to changing the color of the material. A suitable amount of addition of HLA-TiO<sub>2</sub> can render the wallpaper into a natural wood color without unduly damaging the mechanical properties of the material. As shown in Fig. 10, from sample 18 to sample 20, the TS increased from 7.8 to 9.3 MPa, the elongation did not change much and the YM remained at a high level. It is obvious that nanoparticles play a role as the mechanical reinforcement composition, which can especially improve the YM and TS, without affecting considerably the EAB. Some scholars have also discovered similar experimental phenomena (Amin 2012) (Mallakpour and Madani 2015). In their samples, the internal mechanism in the composite is the intercalated/aggregated structure (Chivrac et al. 2010). The nanoparticles fill some of the internal small cracks and are evenly dispersed in the matrix.

However, from samples 21 to 23, many changes have occurred. When the amount of nanoparticles added is too high, the TS and EAB of the composite decrease due to the aggregation of the nanoparticles, which is similar to the experimental conclusions of Amin (Amin 2012) and Norranattrakul

(Norranattrakul et al. 2013). The nanoparticle content is too high, far exceeding the carrying capacity of the plastic matrix, resulting in severe powder agglomeration and exfoliated structure (Chivrac et al. 2010). The exfoliated structure is much less rigid than the intercalated/aggregated structure, which results in a decline in the overall YM of the composite. Among these samples, sample 21 has the best comprehensive mechanical properties (TS 9.4 MPa; EAB 12.3%; YM 2000.1 Mpa).

At a suitable temperature and pressure, lauryl methacrylate containing an unsaturated bond undergoes polymerization and cross-linking reactions under certain external stimulation (Li and Wei 2012; Waguespack et al. 2005). In the twin-screw extruder, lauryl methacrylate is subjected to a shearing force while in high-temperature and high-pressure environment, which makes it prone to cross-link and polymerize. Lauryl methacrylate contains a non-polar long chain and unsaturated bonds which make the polymer and cross-linking product of lauryl methacrylate structurally similar to the plastic matrix (Daugaard et al. 2014). The similar structure let the lauryl methacrylate have a good compatibility with plastic matrix. Lauryl methacrylate can fill small cracks inside the material and bond the filler to the plastic matrix. As shown in Figs. 10 and 13, from sample 24 to sample 29, the erioglaucine disodium salt content of the formulation gradually increased and the color of the sample gradually became darker. The YM of these samples dropped from 2229.5 to 751.2 MPa due to

**Fig. 10** Columnar section drawing of mechanical properties of sample 18 to sample 29





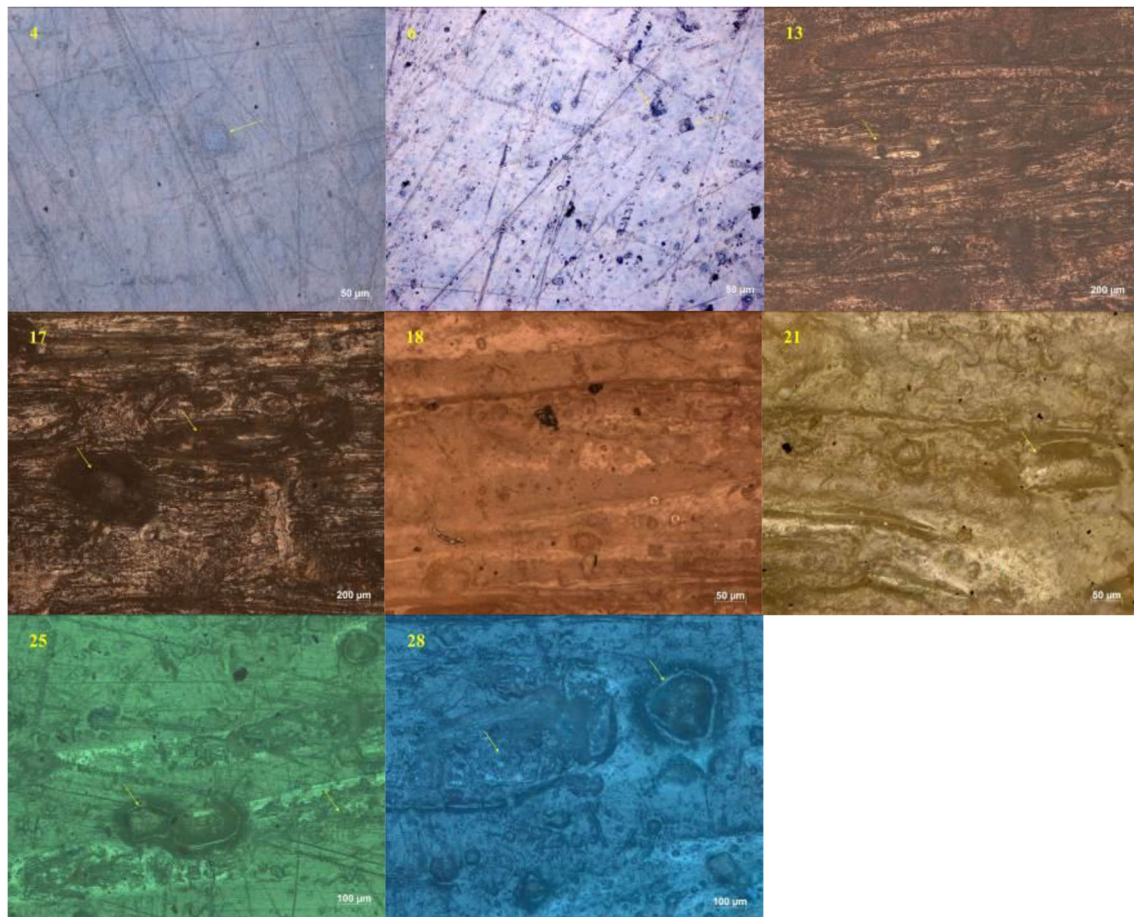


**Fig. 11** Microscopic morphology of several typical samples

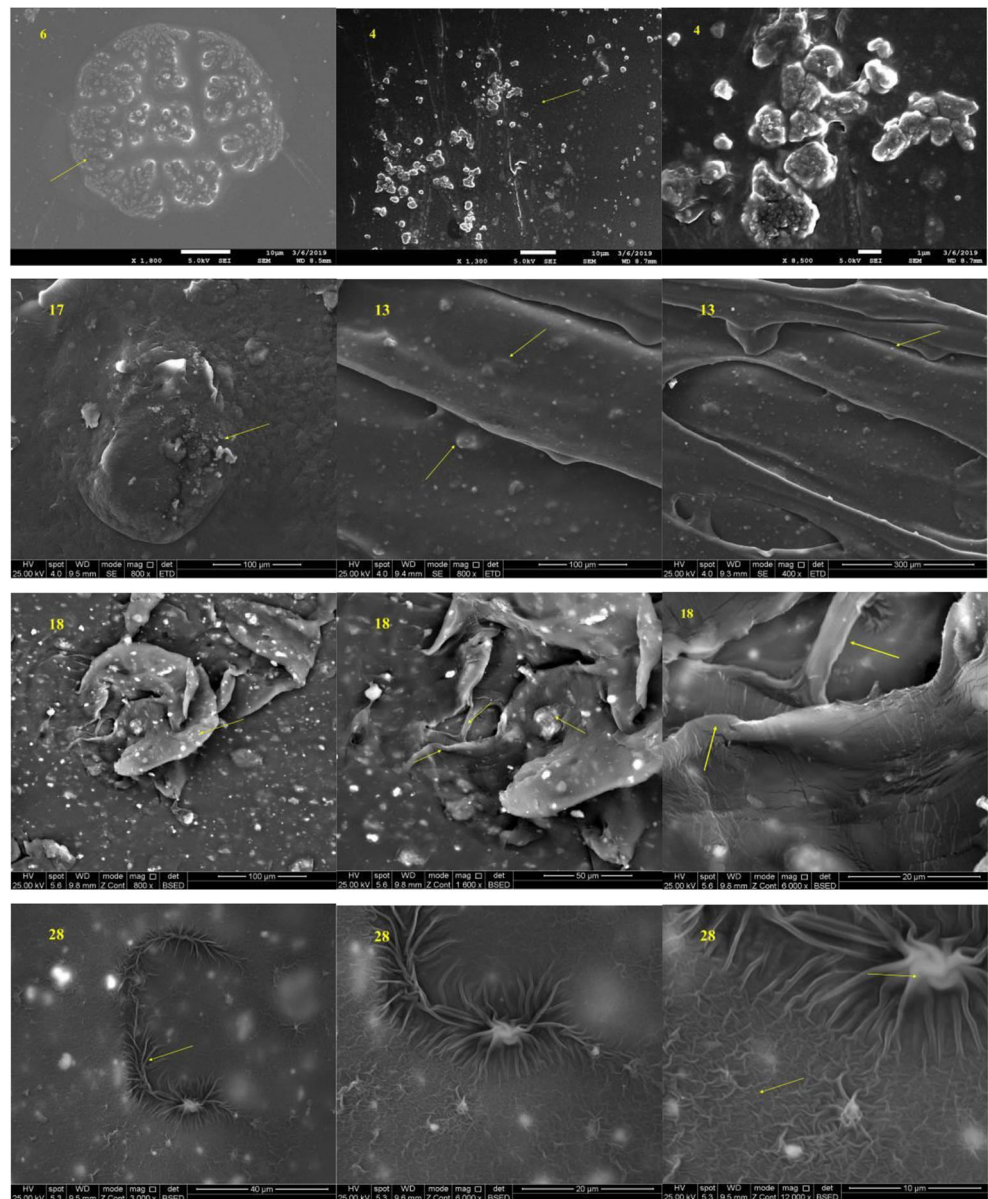
the following reason. The lauryl methacrylate is directly embedded in the plastic matrix after polymerization and cross-linking reaction. As the content of erioglaucone disodium salt increases, more and more erioglaucone disodium salt particles will precipitate from the dye solution during the compounding process, which will damage the adhesion between lauryl methacrylate and the plastic matrix. The TS of these samples decreased from 9.3 to 6.8 MPa and then slightly increased from 6.8 to 7.9 MPa. The EAB from sample 24 to sample 27 remained stable, the EAB of sample 28 rose to 26.6% and sample 29 fell again to 17.9%. In Samples 26 and 27, a certain amount of erioglaucone disodium salt particles were precipitated from the dyeing solution in the cross-linking reaction and polymerization. The connection between the plastic matrix and the cross-linked product was impaired, which caused a decrease in YM. For sample 28, a large amount of erioglaucone disodium salt particles were deposited on the surface of the cross-linked product and polymer network, leaving the network partially detached from the plastic matrix. In this case, the cross-linked product and the polymer are only inserted into the sheet-like structure of the material instead of wrapping it, which in turn causes damage to the original sheet structure. This phenomenon causes some of the fillers to

loosen, resulting in a severe decline in the TS and YM of the material. The detached cross-linked product and polymer network have good ductility and the hindrance to plastic deformation is reduced which make EAB increase, but the overall stiffness of the material is seriously degraded. For sample 29, a severe excess of erioglaucone disodium salt not only disrupts the interface interaction between the network and the plastic matrix but also damages the network itself. Although the erioglaucone disodium salt particles themselves can exert a certain stress transfer effect and the TS is slightly increased, but the clustering of the particles causes a plurality of stress concentration points to appear in the network which lower the EAB. Once partial separation appeared, the cross-linked product and polymer network are inserted directly into the sheet structure, which can cause fatal damage to the overall stiffness of the material. The Sample 29 is not suitable for the development of wallpaper products. The dyeing solvent requires a reasonable concentration.

### Morphological structure analysis

In this article, several typical samples were analyzed using different magnification microscopic morphology. HLA-TiO<sub>2</sub>

**Fig. 12** SEM pictures of several typical samples



nanoparticles are blue in the field of view of the microscope and the place where the HLA-TiO<sub>2</sub> nanoparticles agglomerate is dark blue. As the picture shows, the microscopic morphology of sample 4 is much smoother than that of sample 6. There are some shallow pits and some scratches in the microscopic morphology of sample 4. However, there is a big difference in the microscopic morphology of sample 6. In addition to pits and scratches, there are a large number of messy distribution holes which are deeper. Scratches are caused by the defects of the recycled plastic itself and the shearing force of the screw. The pits and holes are caused by the agglomeration of the HLA-TiO<sub>2</sub> nanoparticles and the uneven mixing of the molten plastic. The formulation of RLDPE and RLLDPE in sample 4 is reasonable. The RLLDPE with short chain branches is not only more ductile but also has a higher MFI. RLLDPE melts

rapidly after being heated and the liquid RLLDPE can encapsulate nanoparticles well. Liquid RLLDPE with good fluidity and ductility can well fill the gaps and holes in the composite, making the nanoparticles more dispersible. This greatly reduces the areas of particle agglomeration and uneven mixing in the composite. The particle agglomeration creates stress concentration points which are prone to fracture. These reasons make the overall mechanical properties of sample 4 better. The microscopic morphology of sample 17 is also very different from the microscopic morphology of sample 13. The relatively wide and deep gaps appeared in the microscopic morphology of sample 17 and its color is darker. Zykova (Zykova et al. 2017) also found a similar microscopic image. As the amount of biomass added increased, the color of the sample gradually deepened and the agglomeration became

more pronounced. In sample 13, the liquefaction filling technology allows the biomass particles to be filled into the plastic matrix in a liquid form, greatly reducing the gaps caused by particle agglomeration. The number of gaps and holes in sample 21 was larger than that of the sample 18, but the color of the sample 21 became light. As a kind of solid staining agent, the addition of HLA-TiO<sub>2</sub> nanoparticles can change the color of the material, but when the amount is too high, serious agglomeration will occur, resulting in many gaps and holes inside the composite. These gaps and holes cause the mechanical properties of the material to deteriorate. Samples 25 and 28 showed green and blue due to the difference in dyeing solvent concentration. The shallow gaps and pits in sample 25 and sample 28 were filled with cross-linked products and polyaddition products of LMA. These places have a scar-like appearance. The deep gaps and pits become shallower after being filled with the polymer and cross-linking product of LMA. The edges of gaps and the pits are the contact areas of the agglomerated particles and the plastic matrix, the interface

interaction at these places is relatively poor. This networked product covers the edges of the gaps and pits, making the filler and plastic connections at the edges tighter.

To further analyze the internal structure of the material, two scanning electron microscopes were used to observe these samples. As showed in Fig. 13 below, the agglomeration problem of nanoparticles in sample 6 is more serious than that in sample 4. The HLA-TiO<sub>2</sub> nanoparticles in the sample 6 agglomerated to form a circular region of regular shape. The HLA-TiO<sub>2</sub> nanoparticles in the composite of sample 4 are dispersed in the plastic matrix and exhibit an irregular distribution as a whole. These circular regions contain more multiple stress concentration points which can cause damage to the mechanical properties of the material. The image difference between sample 17 and sample 13 is particularly large. Both humps and voids are characteristic due to a large amount of agglomeration of the powders inside the material. In addition to the irregular small piles in the image of the sample 17, a large swollen hump appeared. This hump is mainly formed by

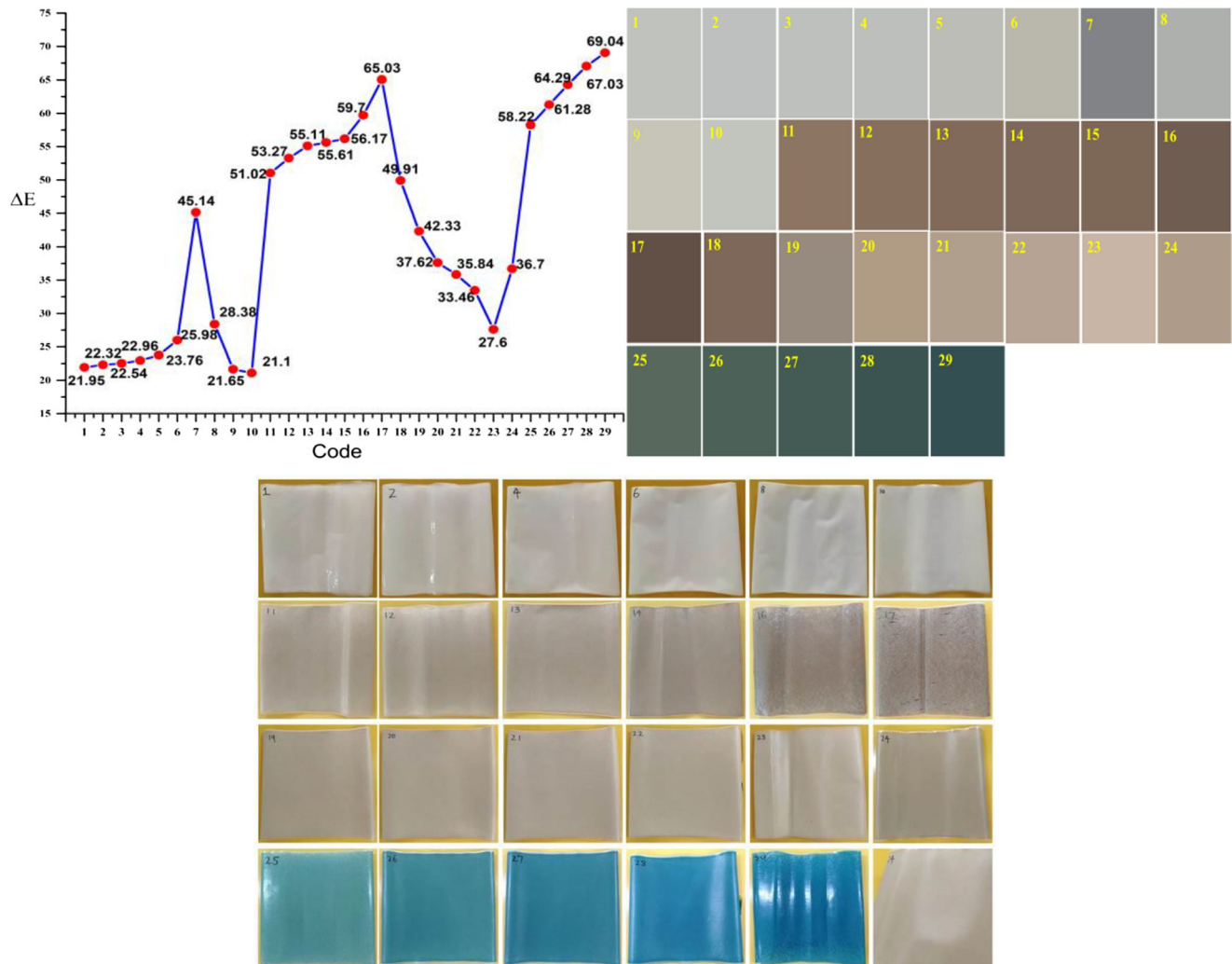


Fig. 13 The physical pictures and chrominance information of the samples

the agglomeration of large particles like biomass powders. The agglomerates of large particle size biomass particles are mixed with a small amount of liquid plastic to form the body of the hump. The agglomerates of small particle size materials such as HLA-TiO<sub>2</sub> nanoparticles particles and ultrafine kaolin are distributed in the internal gaps and surfaces of the hump. Hump and piles both destruct the structural integrity of the matrix and they are harmful to the material. The hybrid created by mixing the liquid biomass filler with a portion of the liquid plastic exhibits a sheet-like structure. These sheet-like structures are widely distributed in the plastic matrix. Some of the hybrids exhibit an irregular neuron-like structure due to unavoidable agglomeration and local differences. These irregular structures are embedded in many sheet structures. The small piles embedded in the sheet-like structure in the Fig. 13 represents this irregular neuron-like structure. The liquid biomass filler and the liquid plastic can be more uniformly mixed due to their similar phase, which greatly reduces the gaps. The liquefaction filling technology not only dissolves cellulose but also dissolves impurities such as hemicellulose, lignin, and pectin. It improves interface interaction between the biomass particles and the hydrophobic plastic matrix. The above reasons result in fewer gaps in the composite and let the sample 13 have better overall mechanical properties. Satapathy (Satapathy and Kothapalli 2018) drew a similar conclusion that filler particles are well dispersed in the RHDPE/BF matrix resulting in fewer flaws and defects. After the composite in sample 18 was subjected to a further compounding process, the internal sheet structure was greatly changed. A part of the sheet-like structures become longer and thinner under the combined action, which exhibit long strip shape. The other part of the sheet-like structures are split and the split structures are adhered to the long strip shape structures to form several kelp-like branch structures. The irregular neuron-like structures also become longer and thinner. The white and bright piles of the sample 18 appear in Fig. 13 represent the grown irregular neuron-like structures which contain more HLA-TiO<sub>2</sub> nanoparticles than the neuron-like structure of sample 13. The new structures in sample 18 are denser than the old structures in the sample 13. The stiffness of the sample 18 is improved due to the more complete fusion process and the long-term synergy of the three mechanical effects.

The feature in sample 28 is the presence of a large number of network structures inside and on the surface of the material. There are two types of network-like structures that appeared in Fig. 13. These network structures exhibit a two-layer distribution. The lower layer network is also the first type of network-like structures, which are a kind of fine fishing net-like network structures created by the polymerization and cross-linking reaction of LMA. The second type of network-like structures are like a neural network in the human body. This kind of network-like structures are distributed on the upper

layer, they are produced by another special process: after the lauryl methacrylate was fused with the grown neuron-like structures in the sample 18, a polymerization and cross-linking reaction occur, thereby new network-like structures are formed by connecting the grown neuron-like structures to each other. The two-layer compound structures fill in tiny cracks in the composite while enhancing the mechanical property of the material. This two-layer compound structures can not only strengthen the interface between the biomass filler and the plastic matrix but also transmit stress well when they are subjected to load. They greatly improve the EAB and TS of the material. Uitterhaegena (Uitterhaegen et al. 2018) also found similar results. The addition of the coupling agent can reduce the disintegration of the interface and facilitate the stress transfer inside the biocomposite material.

### Chroma analysis of materials

The color of the sample is showed in Fig. 14. For the nanoparticle-reinforced matrix, the color difference of the object is difficult to observe with the naked eye. The objects are snowy white, but there is a slight difference in hue and gray. The total color difference of samples 7 and 8 is relatively high, indicating that RLDPE is mixed with some colored impurities during the recycling process. Conversely, sample 9 and sample 10 have a smaller total color difference, indicating that RLLDPE is whiter. The variation of the total color difference from sample 1 to sample 6 indicates that the color of the material can be adjusted by using RLLDPE and nanoparticles. From the analysis of the chroma card, sample 4 has not only better mechanical properties but also better whiteness. From sample 11 to sample 17, the total color difference gradually increases as the content of the biomass component improves. This is because the biomass component is inevitably carbonized when it is heated for a long time. The more biomass components, the more carbonized biomass components, the deeper the color of the material. The analysis of physical photographs reveals that excessive biomass levels have two additional side effects in addition to deepening the color of the material. One is that the powder agglomerates on the surface of the material, resulting in a very rough surface. The other is that powder agglomeration leads to small holes and flaws on the surface of the material. This problem is particularly severe in sample 17 and this problem of sample 18 is mitigated by the application of liquid filling technology. Sample 13 has not only good mechanical properties but also a color in a suitable range. From sample 18 to sample 23, the total color difference of the material gradually decreased. The addition of the HLA-TiO<sub>2</sub> nanoparticles can improve the color of the material, but not as much as possible. Although excessive HLA-TiO<sub>2</sub> nanoparticles give the material a good whiteness,

they can impair the mechanical properties of the material and increase the surface roughness of the material. Sample 23 has such a problem. Sample 21 having a relatively good overall performance can be developed by adding an appropriate amount of HLA-TiO<sub>2</sub> nanoparticles. Sample 24, which was developed on the basis of sample 21, showed no significant change in the total color difference. This indicates that the cross-linking reaction and polymerization of LMA do not have a large effect on the color of the material. Sample 24 has the color of pear wood and its mechanical properties were also improved. It is an ideal material for making wood color wallpapers. From sample 25 to sample 29, as the concentration of the dye solution increases, the total color difference of the material gradually increases. Through a comprehensive analysis of physical pictures and chroma cards, it was found that samples 26 and 28 are the rational materials for the development of green and blue wallpapers, respectively. The green color of sample 25 is accompanied by a certain yellow hue, the color of sample 27 is between green and blue. The concentration of the dye solution of sample 29 is too high resulting in the unnecessary increase in cost and the decline of material mechanical properties.

### Feasibility analysis of dyes

The feasibility of a suitable dye is very important for the dyeing process of wallpaper. Pigments such as anthocyanins and chlorophyll extracted from natural plants have good affinity with biomass components and are not toxic to humans. But high cost makes it unsuitable for wallpaper development. Azo dyes and metal complex dyes are widely used in industry, but they have some problems. Aromatic amines produced by the metabolism can cause various malignant tumors such as liver cancer (Feng et al. 2012) (Chung 2016) when the azo dye entered the human body through the esophagus and skin mucosa. The discarded product contained metal complex dyes will bring the heavy metals to the soil and water bodies, seriously damaging the ecological environment. Erioglaucine disodium salt is one of the common food colors. It not only has a certain affinity with biomass but also is non-toxic and environmentally friendly. According to the data provided by Macleans Co., Ltd. (Shanghai, China), the purchase of the same weight of 25 g of raw materials, erioglaucine disodium salt costs 72 yuan, chlorophyll costs 426 yuan, while anthocyanin costs 844.50 yuan. The erioglaucine disodium salt used in this paper is economical. The erioglaucine disodium is in powder form at normal temperature and its melting point is 100 °C. These performances let it have the advantages of convenient addition and easy to melt. As a kind of solid dye, nano titanium dioxide has two main crystalline forms: anatase

and rutile. There are three types of anatase-type titanium dioxide: hydrophilic and lipophilic anatase-type titanium dioxide, hydrophilic anatase-type titanium dioxide, and lipophilic anatase-type titanium dioxide. The hydrophilic and lipophilic anatase-type titanium dioxide has a good compatibility with the biomass component containing abundant hydroxyls and the cross-linking agent containing ester group. HLA-TiO<sub>2</sub> has a higher reflectance in the short-wave portion of visible light than rutile-type titanium dioxide, so it exhibits a blue hue in the above picture. The HLA-TiO<sub>2</sub> not only reduces the formaldehyde generated during decoration and improves the environmental friendliness of the wallpaper due to its high photo catalytic activity but also gives the wallpaper a certain degree of self-cleaning ability. The free radicals with strong photooxidation are generated by anatase-type titanium dioxide that exposed to sunlight, which can cause the catalyze photolysis of various organic substances such as formaldehyde, oil stains, and bacteria on the surface of the wallpaper. These substances will be converted into gasses or substances that can be easily rubbed off.

### Conclusions

The wallpaper product developed in this article is in conformity with the concept of plastic recycling economy and the sustainable development of agriculture. A complete set of process system and theories of Liquefaction filling technology and hybrid network model construction technology are proposed. Based on the results of characterization, this paper proposes a specific 3D model of material formation mechanism. The experiment found that the matrix products with the reasonable RLDPE and RLLDPE ratio (1:0.26) have good particle stress transfer effect and good comprehensive mechanical properties (TS 11.4 MPa; EAB 309.3%; YM 499 MPa). The reasonable ratio of biomass to specialty solvents is 1:1.5. The product developed based on this ratio has excellent filler dispersion, good filler/matrix interface, and good comprehensive mechanical properties (TS 8.009 MPa; EAB 28.2%; YM 1263.1 Mpa). When the solid dye is additionally added at 15 g, the sample has not only good whiteness ( $\Delta E = 35.84$ ) but also the best mechanical properties (TS 9.406 MPa; EAB 12.3%; YM 2000.1 Mpa). The reasonable concentration of the dye solution for the development of the pear wood color wallpaper product ( $\Delta E = 36.7$ ), the green wallpaper product ( $\Delta E = 61.28$ ), and the blue wallpaper product ( $\Delta E = 67.03$ ) is 0%, 0.99%, and 2.91%, respectively. The two-layer network structure produced by cross-linking reaction and polymerization can improve the mechanical properties of the material such as the wood-colored wallpaper. Its TS is 9.255 MPa, the EAB is 20.998%, and the YM is 2229.475 MPa.

## References

- Amin KAM (2012) Reinforced materials based on chitosan, TiO<sub>2</sub> and Ag composites. *Polymers* 4(1):590–599. <https://doi.org/10.3390/polym4010590>
- Arena M, Abbate C, Fukushima K, Gennari M (2011) Degradation of poly (lactic acid) and nanocomposites by *Bacillus licheniformis*. *Environ Sci Pollut Res* 18(6):865–870. [https://doi.org/10.1007/978-3-642-37916-1\\_30](https://doi.org/10.1007/978-3-642-37916-1_30)
- Barnes SJ (2019) Understanding plastics pollution: the role of economic development and technological research. *Environ Pollut*. <https://doi.org/10.1016/j.envpol.2019.03.108>
- Bhagat VK, Biswas S, Dehury J (2014) Physical, mechanical, and water absorption behavior of coir/glass fiber reinforced epoxy based hybrid composites. *Polym Compos* 35(5):925–930. <https://doi.org/10.1002/pc.22736>
- Cano L, Pollet E, Avérous L, Tercjak A (2017) Effect of TiO<sub>2</sub> nanoparticles on the properties of thermoplastic chitosan-based nanobiocomposites obtained by mechanical kneading. *Compos A: Appl Sci Manuf* 93:33–40. <https://doi.org/10.1016/j.compositesa.2016.11.012>
- Cao G, Zhang X, Wang Y, Zheng F (2008) Estimation of emissions from field burning of crop straw in China. *Chin Sci Bull* 53(5):784–790 CNKI:SUN:JXTW.0.2008-05-023
- Cecchi T, Giuliani A, Iacopini F, Santulli C, Sarasini F, Tirillò J (2019) Unprecedented high percentage of food waste powder filler in poly lactic acid green composites: synthesis, characterization, and volatile profile. *Environ Sci Pollut Res* 26(7):7263–7271. <https://doi.org/10.1007/s11356-019-04187-1>
- Chatterjee S, Sharma S (2019) Microplastics in our oceans and marine health. *Field actions science reports*. *J Field Actions (Special Issue 19)*:54–61
- Cheranov O, Arterburn L, Centeno D, Feuerborn L, Min H, Penrod C et al (2019) Explorations of polyethylene terephthalate (PET) hydrolase for addressing PET plastic pollution. *The FASEB Journal* 33(1\_supplement):lb211–lb211
- Chivrac F, Pollet E, Dole P, Avérous L (2010) Starch-based nanobiocomposites: plasticizer impact on the montmorillonite exfoliation process. *Carbohydr Polym* 79(4):941–947. <https://doi.org/10.1016/j.carbpol.2009.10.018>
- Chung K-T (2016) Azo dyes and human health: a review. *J Environ Sci Health, Part C* 34(4):233–261. <https://doi.org/10.1080/10590501.2016.1236602>
- Clemons C (2002) Wood-plastic composites in the United States: the interfacing of two industries. *For Prod J* 52(6):10. [https://doi.org/10.1016/S1389-9341\(02\)00014-X](https://doi.org/10.1016/S1389-9341(02)00014-X)
- d'Ambrières W (2019) Plastics recycling worldwide: current overview and desirable changes. *Field actions science reports*. *J Field Actions (special issue 19)*:12–21
- Daugaard AE, Jankova K, Hvilsted S (2014) Poly (lauryl acrylate) and poly (stearyl acrylate) grafted multiwalled carbon nanotubes for polypropylene composites. *Polymer* 55(2):481–487. <https://doi.org/10.1016/j.polymer.2013.12.031>
- Defruyt S (2019) Towards a new plastics economy. *Field actions science reports*. *J Field Actions (special issue 19)*:78–81
- Fangfang D, Zhang M, Jingping W (2011) Preparation and properties of corn stalk fiber/PBS composite. *Polym Mater Sci Eng* 27(10):41
- Feng J, Cerniglia CE, Chen H (2012) Toxicological significance of azo dye metabolism by human intestinal microbiota. *Front Biosci (Elite edition)* 4:568–586. <https://doi.org/10.2741/400>
- Gao D, Chang J, Gong X (2007) Research on corn straw cushion packaging material [J]. *Packag Eng* 1
- Ge ZH, Si DG, Lan YL, Shi MN. (2017). The effect of modifying agents on the mechanical properties of straw flour/waste plastic composite materials. Paper presented at the Key Engineering Materials
- Guo F, Aryana S, Han Y, Jiao Y. (2018). A review of the synthesis and applications of polymer–nanoclay composites (Vol. 8)
- Jain N, Bhatia A, Pathak H (2014) Emission of air pollutants from crop residue burning in India. *Aerosol Air Qual Res* 14(1):422–430 aaqr.2013.01.0031
- Kaymakci A, Ayırlıms N (2014) Investigation of correlation between Brinell hardness and tensile strength of wood plastic composites. *Compos Part B* 58:582–585. <https://doi.org/10.1016/j.compositesb.2013.11.009>
- Ku H, Wang H, Pattarachaiyakop N, Trada M (2011) A review on the tensile properties of natural fiber reinforced polymer composites. *Compos Part B* 42(4):856–873. <https://doi.org/10.1016/j.compositesb.2011.01.010>
- Li S, Wei J (2012) Evaluation of the influence of homopolymerization on the removal of water-insoluble organics by grafted polypropylene fibers. *Mar Pollut Bull* 64(6):1172–1176. <https://doi.org/10.1016/j.marpolbul.2012.03.021>
- Lin Z, Zhuang L, LI-juan A, Jiang C, Jing L, Jun W, et al. (2011) Preparation condition optimization of corn stalk fiber cushioning material. *Packag Eng* 7. <https://doi.org/10.3354/cr00999>
- Liu R, Peng Y, Cao J, Chen Y (2014) Comparison on properties of lignocellulosic flour/polymer composites by using wood, cellulose, and lignin flours as fillers. *Compos Sci Technol* 103:1–7. <https://doi.org/10.1016/j.compscitech.2014.08.005>
- Lowa JH, Andenana N, Rahman W, Rusmana R, Majida RA (2017) Evaluation of rice straw as natural filler for injection molded high density polyethylene bio-composite materials. *Chem Eng Trans* 56: 1081–1086. <https://doi.org/10.3303/CET1756181>
- Mallakpour S, Madani M (2015) Effect of functionalized TiO<sub>2</sub> on mechanical, thermal and swelling properties of chitosan-based nanocomposite films. *Polym-Plast Technol Eng* 54(10):1035–1042
- Miller S, Billington S, Lepech M (2013) Improvement in environmental performance of poly (β-hydroxybutyrate)-co-(β-hydroxyvalerate) composites through process modifications. *J Clean Prod* 40:190–198
- Nagarajan V, Misra M, Mohanty AK (2013) New engineered biocomposites from poly (3-hydroxybutyrate-co-3-hydroxyvalerate) (PHBV)/poly (butylene adipate-co-terephthalate) (PBAT) blends and switchgrass: fabrication and performance evaluation. *Ind Crop Prod* 42:461–468. <https://doi.org/10.1016/j.indcrop.2012.05.042>
- Njoku R, Ofili I, Agbiogwu D, Agu C (2012) Effect of alkali treatment and fiber content variation on the tensile properties of coir fiber reinforced cashew nut shell liquid (CNSL) composite. *Niger J Technol* 31(2):108–110
- Norranattrakul P, Siralertmukul K, Nuisin R (2013) Fabrication of chitosan/titanium dioxide composites film for the photocatalytic degradation of dye. *J Met Mater Miner* 23(2)
- Özmen N (2012) A study of the effect of acetylation on hemp fibres with vinyl acetate. *BioResources* 7(3):3800–3809
- Patel B, Acharya S, Mishra D (2012) Environmental effect of water absorption and flexural strength of red mud filled jute fiber/polymer composite. *Int J Eng Sci Technol* 4(4):49–59. <https://doi.org/10.4314/ijest.v4i4.5>
- Pothan LA, Thomas S, Neelakantan N (1997) Short banana fiber reinforced polyester composites: mechanical, failure and aging characteristics. *J Reinf Plast Compos* 16(8):744–765
- Qu C, Li B, Wu H, Giesy JP. (2012). Controlling air pollution from straw burning in China calls for efficient recycling: ACS publications
- Saba N, Tahir P, Jawaid M (2014) A review on potentiality of nano filler/natural fiber filled polymer hybrid composites. *Polymers* 6(8):2247–2273. <https://doi.org/10.3390/polym6082247>
- Satapathy S, Kothapalli RV (2018) Mechanical, dynamic mechanical and thermal properties of banana fiber/recycled high density polyethylene biocomposites filled with flyash cenospheres. *J Polym Environ* 26(1):200–213. <https://doi.org/10.1007/s10924-017-0938-0>

- Sreekumar PA, Joseph K, Unnikrishnan G, Thomas S (2007) A comparative study on mechanical properties of sisal-leaf fibre-reinforced polyester composites prepared by resin transfer and compression moulding techniques. *Compos Sci Technol* 67(3):453–461. <https://doi.org/10.1016/j.compscitech.2006.08.025>
- Tajeddin B, Ansari H (2017) The effect of wheat straw bleaching on the some mechanical properties of wheat straw/LDPE biocomposites. *J Food Bioprocess Eng* 2(2):1–9
- Uitterhaegen E, Parinet J, Labonne L, Mérian T, Ballas S, Véronèse T et al (2018) Performance, durability and recycling of thermoplastic biocomposites reinforced with coriander straw. *Compos A: Appl Sci Manuf* 113:254–263. [j.compositesa.2018.07.038](https://doi.org/10.1016/j.compositesa.2018.07.038)
- Waguespack BL, Hodges SA, Bush ME, Sondergeld LJ, Bushey MM (2005) Capillary electrochromatography column behavior of butyl and lauryl acrylate porous polymer monoliths. *J Chromatogr A* 1078(1–2):171–180. <https://doi.org/10.1016/j.chroma.2005.04.083>
- Wang C. (2001). Method for manufacturing packaging material and sheets from plant straws: Google patents
- Wang G, Kawamura K, Xie M, Hu S, Cao J, An Z, Waston JG, Chow JC (2009) Organic molecular compositions and size distributions of Chinese summer and autumn aerosols from Nanjing: characteristic haze event caused by wheat straw burning. *Environ Sci Technol* 43(17):6493–6499. <https://doi.org/10.1021/es803086g>
- Wei F, Zhang L, Pang Z, Guo S (2011) The economic and environmental analysis of crop residues burning and reutilization in China. *Chin Agric Sci Bull.* [https://doi.org/10.1016/S1671-2927\(11\)60313-1](https://doi.org/10.1016/S1671-2927(11)60313-1)
- Xiue LTJ (2003) Effects of crop straw burning on soil organic matter and soil microbes [j]. *Soils* 4:16
- Yang Chunhe BX (2005) Wo Fei agricultural waste pollution and prevention countermeasures. *Agric Environ Dev* 2008:2115–2118
- Yang G, Wang Y, Zeng Y, Gao GF, Liang X, Zhou M et al (2013) Rapid health transition in China, 1990–2010: findings from the global burden of disease study 2010. *Lancet* 381(9882):1987–2015. [https://doi.org/10.1016/S0140-6736\(13\)61097-1](https://doi.org/10.1016/S0140-6736(13)61097-1)
- Yin Z. (2013). Straw plastic and preparation method thereof: Google patents
- Zhang Y, Zang G-Q, Tang Z-H, Chen X-H, Yu Y-S (2014) Burning straw, air pollution, and respiratory infections in China. *Am J Infect Control* 42(7):815. <https://doi.org/10.1016/j.ajic.2014.03.015>
- Zykova A, Pantyukhov P, Popov A (2017) Ethylene–octene copolymer–wood flour/oil flax straw biocomposites: effect of filler type and content on mechanical properties. *Polym Eng Sci* 57(7):756–763. <https://doi.org/10.1002/pen.24626>

**Publisher's note** Springer Nature remains neutral with regard to jurisdictional claims in published maps and institutional affiliations.